Cerebellar output shapes cortical preparatory activity during motor adaptation

Sharon Israely*[1], Hugo Ninou*[1,2,3], Ori Rajchert[4], Lee Elmaleh[1], Ran Harel[5], Firas Mawase[4], Jonathan Kadmon[¥1], Yifat Prut[¥1]

*These authors contributed equally to this work.

[1] The Edmond and Lily Safra Center For Brain Sciences, The Hebrew University, Jerusalem, 91904-01, Israel
[2] Laboratoire de Neurosciences Cognitives et Computationnelles, INSERM U960, Département D'Etudes Cognitives, Ecole Normale Supérieure, PSL University, Paris, France
[3] Laboratoire de Physique de l'Ecole Normale Superieure, Ecole Normale Supérieure, PSL University, Paris, France
[4] Faculty of Biomedical Engineering, Technion - Israel Institute of Technology, Haifa, Israel
[5] Department of Neurosurgery, Sheba Medical Center, 5262000 Tel Aviv, Israel

[¥]These authors contributed equally. Co-correspondence: yifat.prut@mail.huji.ac.il and jonathan.kadmon@mail.huji.ac.il

Abstract

The cerebellum plays a key role in motor adaptation by driving trial-to-trial recalibration of movements based on previous errors. In primates, this adaptive response is achieved by cerebellar modulation of motor cortical signals, but the nature and timing of this process are unknown. Specifically, cortical correlates of adaptation are encoded already in the pre-movement motor plan, but these early cortical signals could be driven by a cerebellar-to-cortical information flow or evolve independently through intracortical mechanisms. To address this question, we trained monkeys to reach against a viscous force field while blocking cerebellar outflow. During the force field trials, the cerebellar block led to impaired adaptation and a compensatory, re-aiming-like shift in motor cortical preparatory activity. In the null-field conditions, the cerebellar block altered neural preparatory activity by increasing task-representation dimensionality and impeding generalization. A computational model indicated that low-dimensional (cerebellar-like) feedback is sufficient to replicate these findings. We conclude that cerebellar signals carry task structure information that constrains the dimensionality of the cortical preparatory manifold and promotes generalization. In the absence of these signals, cortical mechanisms are harnessed to partially restore adaptation.

Main

Motor adaptation is a remarkable mechanism utilized by all living beings to adjust to changes in both the external environment and the internal physiological state, an ability which supports routine behavior and long-term survival[1,2]. Numerous studies have shown that motor adaptation is achieved by tuning an internal model of the limbs[3,4]. In vertebrates, the cerebellum is considered to be the site where internal models are stored and is therefore responsible for the trial-by-trial recalibration of motor commands[5-8]. This assumption is supported by considerable data from animal models[9-11], imaging studies[12], and observations of cerebellar patients[13-18] who have difficulties adapting to novel environments. However, the mechanisms by which the

cerebellar-based internal model gains access to motor output during sensorimotor adaptation remain unclear.

In the upper limb system of humans and nonhuman primates, cerebellar signals are predominantly relayed through the motor thalamus to the motor cortex[19], suggesting that adaptive motor behavior evolves through cerebellar-to-cortical interactions. Consistent with this view, large parts of the sensorimotor network, including the motor, premotor and somatosensory cortices[20-25] have been shown to correlate with motor learning as early as the planning phase of movements[22,26]. These early signals may have evolved through intra-cortical mechanisms to integrate with cerebellar signals when movements begin. Alternatively, adaptation-related cortical signals might reflect pre-movement cerebellar-to-cortical interactions that occur during this time [27-29].

Here, we aimed to delineate the cerebellar contribution to motor adaptation by training monkeys to reach against a velocity-dependent force field while cerebellar output was reversibly blocked[30]. Blocking cerebellar signals resulted in a significantly impaired adaptation, consistent with observation in cerebellar patients[31,32]. The impaired motor behavior was preceded by changes in pre-movement neural activity, characterized by a rotational shift in neural state, and a significant increase in the dimensionality of activity compared to control conditions. Finally, under these circumstances, across-target generalization was impaired at the neural and behavioral levels. A computational model explained these findings by showing that low-dimensional (cerebellar-like) feedback is sufficient to quench the dimensionality of the cortical manifold, thereby improving its generalization performance. These results suggest a dual role for cerebellar signals in motor adaptation. Firstly, these signals translate preparatory cortical activity into adapted motor output and their absence triggers cortical compensatory mechanisms that are evident already during motor preparation. Secondly, cerebellar signals constrain cortical preparatory activity into a low-dimensional manifold by introducing the task-structure information needed for generalization both at the neural and behavioral levels.

Results

Cerebellar block impairs force field adaptation

We trained two monkeys to wear an exoskeleton (Kinarm system) and perform an instructed delay center-out planar reaching task. The two monkeys were implanted with a chronic stimulation electrode in the superior cerebellar peduncle (SCP), which was used to block the outflow of cerebellar signals by applying high-frequency stimulation (HFS), as reported in detail elsewhere[30]. The task design (**Fig. 1a,b**) consisted of four different task conditions: two pre-learning conditions with and without cerebellar outflow block (termed control and HFS, respectively), and two force-field learning epochs (termed FF and FF-HFS respectively). During the control trials, the monkeys were able to maintain straight trajectories towards the presented target (**Fig. 1c**). In the presence of HFS, the trajectories became more variable, as quantified by their maximal deviation from a straight line (t-test: $p = 0.00072$ Monkey P, $p=2.1871e-10$ Monkey S). Figure 1d presents trajectories of movements during a single FF adaptation session and the effect of adding HFS on adaptation. In both cases, the FF caused deviations in arm trajectories, but when the FF adaptation was combined with HFS, the trajectories were substantially more variable, even though the monkeys were able to reduce the error and converge to a partially-adapted state (similar to cerebellar patients[31]). The trajectory errors caused by the FF were quantified by measuring the vertical distance from the shortest (straight) path connecting the initiation and end points of the performed trajectory. The error was measured at two time points along the trajectory: an early time point (150 ms after movement onset), at which feedback was not yet available, and the time of maximal deviation. Figure 1d depicts the learning curves during FF (blue traces) and during FF-HFS (red traces) as measured at the early (left panel) and late (right panel) time points of the trajectories. In both conditions, learning was initially fast and replaced by a

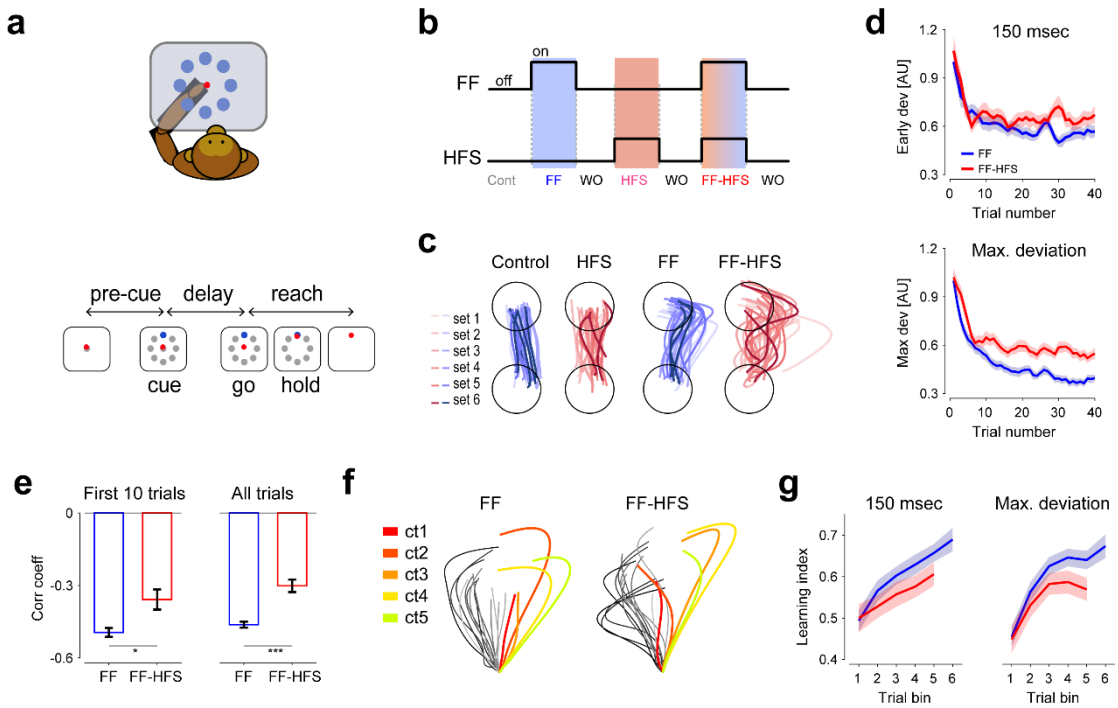

Figure 1. Experimental setup and behavioral results. a, Behavioral paradigm. Monkeys were trained to wear an exoskeleton and control a cursor that appeared on a horizontally positioned screen. The movements of the monkeys were constrained to planar, shoulder-elbow reaching movements. The sequence of events composing a single trial included a pre-cue period until the appearance of the peripheral target, a delay period, and a 'go' signal (removal of the central target), after which the monkey had to acquire the target within a limited response time. Correct performance resulted in a reward (a drop of applesauce). **b,** Sequence of conditions composing a single session, including control (Cont.) trials, force field (FF) trials, washout (WO), and HFS trials. Blue and/or red shadings indicate the start of FF and/or HFS. **c,** Hand trajectories in each of the four conditions (±FF and ±HFS). Color hues of each trajectory correspond to the time during the session in which the specific trajectory was performed (dark hues = later trials). **d,** Mean deviation of the hand trajectory from the shortest (straight) line connecting the initial and the end position as a function of trial number during FF sessions in the control (blue) and HFS (red) trials. Deviations were computed at 150 ms after movement onset (left) and at the point of maximal deviation (right). Single session data were normalized (see Methods) and deviations are shown in arbitrary units. **e,** Correlation coefficients between trial number and maximal deviations calculated for each adaptation session (using the first 10 trials of the session – left panel or all trials – right panel) and averaged over all sessions. **f,** Trajectory samples taken from a single session during FF (left) and FF-HFS (right) conditions. Color-coded trajectories highlight the catch trials that were interleaved between FF trials (gray trajectories - dark to light shadings correspond to early to late trials, respectively). The color of the catch trial trajectories corresponds to the time in the session in which trials were inserted on a red-to-green scale (red - early trials, green - late trials). **g,** Learning index of catch trials plotted as a function of the trial bin (groups of 10 trials) for deviations calculated at 150 ms after movement onset (left) and maximal deviations (right). FF trials are shown in blue and FF-HFS in red.

slower learning phase after about 10 trials. In terms of maximal deviation, both phases of adaptation were impaired by the HFS (2- way ANOVA, HFS effect, p=4.04e-56; trial number effect, p=4.18e-97, Interaction effect, p=2.4e-4).

In addition to the increased residual error, the adaptation itself was more variable under HFS, as measured by trial-to-trial reduction in trajectory errors during learning. To quantify this effect, for each adaptation session, we correlated the error size and

111 trial number. This measure captured the tendency for error reduction across trials in
112 each adaptation session. There were significantly lower correlation values under HFS,
113 indicating a more erratic convergence to the adapted state (**Fig. 1e**, Wilcoxon rank
114 sum test: $p<0.05$, $p<0.0001$ left and right panels, respectively). Finally, the significantly
115 impaired adaptation under HFS was demonstrated using catch trials, where the FF was
116 unexpectedly removed (**Fig. 1f**). Catch trials are used to expose the underlying learning
117 achieved during adaptation trials[33]. The learning index, calculated using the catch
118 trials (see Methods), was divided into bins of 10 trials each (**Fig. 1g**). In the presence
119 of HFS, the learning index was significantly lower than in the control trials (2-way
120 ANOVA, HFS effect: $p = 0.0365$, Time bin effect $p = 0.0089$ for the deviation measured
121 at 150; HFS effect $p = 0.0028$ and Time bin effect $p = 0.0018$ for maximal deviation).
122 This lower learning index further confirmed the observed impaired adaptation when
123 cerebellar signals were blocked.

124 **Blocking cerebellar outflow decreased error sensitivity and increased internal noise**

125 The efficiency of motor adaptation is driven by two opposing processes: *error*
126 *sensitivity*, which measures the extent of learning from previous errors, and the
127 *retention factor*, which quantifies the ability of the system to retain the newly acquired
128 motor skill[2,34,35]. We calculated these two measures from our data (see Methods
129 section) and found that under HFS, the error sensitivity decreased, on average, by 22%
130 (paired t-test, $p<0.0001$) whereas the retention factor decreased by 5% (paired t-test
131 $p<0.005$), suggesting that the impaired adaptation under HFS is mostly driven by
132 impaired learning from previous errors (**Fig. 2a,b**).

133 Next, we explored which mechanisms were most likely related to the decrease in error
134 sensitivity under HFS. Error sensitivity is strongly affected by execution noise through
135 its relationship to error size and error consistency. Behavioral studies have shown that

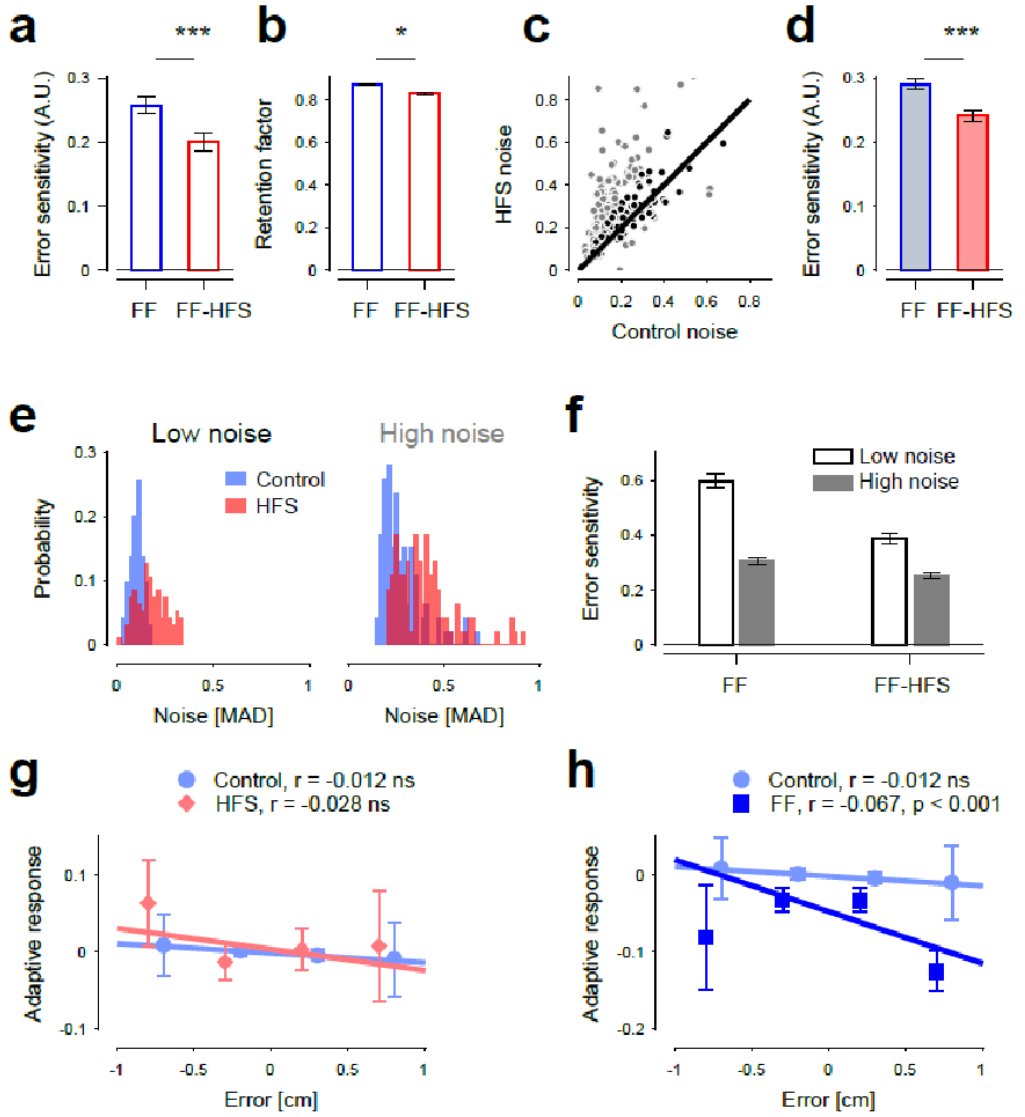

Figure 2. Effect of HFS on adaptation rate. a, Error sensitivity during adaptation for FF (blue) and FF-HFS (red) conditions, averaged over all sessions. **b,** Average retention factors. **c,** Single-session motor noise was estimated by calculating the mean absolute deviation (MAD) of maximal deviations during HFS trials and plotting against the motor noise calculated during the matching control sessions. Darker dots indicate sessions where the motor noise under HFS was comparable to the motor noise level during the control trials (i.e., HFS/Control ratio > 0.6 and < 1.4). **d,** Error sensitivity calculated for a subset of adaptation sessions, for which the pre-adaptation noise level was comparable during FF (blue) and FF-HFS (red) conditions (i.e., highlighted sessions in panel c). **e,** Distribution of motor noise in each session during the control (blue) and HFS conditions (red) for low (left) and high (right) noise levels. Sessions were split into low-noise and high-noise sessions based on the median noise level (see Methods). **f,** Error sensitivity in low-noise (white bars) and high-noise (gray bars) sessions (as defined using the control and HFS trials) and calculated in the FF and FF-HFS conditions. **g,** Adaptive response, quantified by the difference in maximal deviation between trial n+1 and n-1, regressed onto the deviation on n-th trial (i.e., Error). **h,** Same as g, for the adaptive response in the FF conditions, and compared to control.

repeated exposure to inconsistent errors (i.e., errors that fluctuate in polarity around the mean trajectory[36]), or variable perturbations (i.e., irregular cursor-to-hand angular deviations on a visuomotor rotation task[37]) lead to a reduction in error sensitivity and

139 impaired adaptation. It is, therefore, conceivable that the drop in error sensitivity
140 under HFS was simply the outcome of the increased movement variability in these
141 conditions. To address this possibility, we estimated the conditioning-specific motor
142 noise by calculating the variability of the trajectory errors (i.e., the variance of the
143 maximal deviation values) in the pre-learning conditions (i.e., during control and HFS
144 trials). The results showed that under HFS, motor noise was significantly higher than
145 in the control trials (**Fig. 2C**, paired t-test, $p < 0.0001$).

146 Nevertheless, the added execution noise under HFS could not fully account for the
147 reduced error sensitivity. To show this, we first selected sessions with similar levels of
148 noise during the control and HFS trials and measured the error sensitivity during FF
149 and FF-HFS adaptation sessions. Figure 2c depicts a selected subset of sessions with
150 matched noise levels (at a ratio of 0.6 to 1.4 between the corresponding noise levels),
151 and Figure 2d presents the mean error sensitivity calculated for this subset. We found
152 that during FF-HFS, error sensitivity was significantly lower than in the FF trials (paired
153 t-test, $p < 0.0001$) even though the noise levels were comparable.

154 In addition, the sheer magnitude of the noise level (irrespective of the similarity in
155 noise level between control and HFS) was also unable to explain the changes in error
156 sensitivity during HFS. This was demonstrated by classifying the recording sessions
157 into low or high levels of noise (**Fig. 2e**) and then calculating the mean error sensitivity
158 in 4 (2x2) different conditions: low/high noise x FF/FF-HFS (**Fig. 2f**). We found that
159 error sensitivity was generally higher at low vs. high levels of noise, but within each
160 noise level category, the error sensitivity was significantly lower in the presence of HFS
161 (**Fig. 2f**, results for the two monkeys pooled, HFS effect: p=5.47e-13, noise level effect:
162 p=3.72e-32, Interaction effect: p=1.41e-4).

163 Finally, motor noise is often categorized as either internal (i.e., execution noise) or
164 external (a consequence of external interferences in the environment). Since external
165 (but not internal) noise reduces error sensitivity[37] , it was crucial to identify whether
166 the added motor noise in the HFS trials was treated as an external noise that will
167 trigger a corrective (adaptive) response in subsequent trials or an internal source of
168 noise that will be ignored. Using this approach, we found no adaptive response under

169 HFS (in the absence of FF), as evidenced by the lack of correlation between the error
170 size on a given HFS trial and the change in error between flanking trials (**Fig. 2g**,
171 regression slope in control -0.012, n.s.; regression slope in HFS -0.028, n.s.), whereas
172 FF produced a significant adaptive response (**Fig. 2h**, regression slope in control -0.012
173 n.s.; regression slope in FF -0.067 p=4.38e-06). This result suggests that HFS likely acts
174 as an internal noise source, affecting adaptation by mechanisms other than the
175 addition of an external (i.e., perceivable) noise source.

176 Taken together, these results suggest that the impaired adaptation during HFS was
177 driven by two (at least partially) independent processes: decreased error sensitivity
178 and increased internal noise.

179 **The cerebellar block induced target-independent and target-specific changes in the**
180 **preparatory cortical state**

181 We recorded neural activity from the primary and premotor cortical areas during task
182 performance and tested the effects of FF and/or HFS on cell activity (**Fig. 3a**). At the
183 population level, the cerebellar block led to a decrease in the task-related modulation
184 of firing rates, measured by comparing the maximal rate modulation in HFS to the
185 control (**Fig. 3b**, paired t-test, n=218 $p < 3.02e-6$ for both monkeys, $p < 2e-3$ for
186 monkey P and $p < 5.4e-3$ for monkey S). The effect of HFS was apparent even before
187 the "Go" signal during the preparatory period, suggesting that cerebellar output
188 affects motor cortical firing even before movement starts. Since previous studies
189 showed that motor adaptation is accompanied by changes in the coordinated activity
190 of motor cortical neurons during motor preparation [Vyas et al., 2020, Sun et al., 2022]
191 , we tested whether cerebellar signals are involved in recalibrating movement by
192 shaping motor cortical preparatory activity in a task-dependent manner. To do so, we
193 first applied dimensionality reduction methods on the pre-learning dataset to identify
194 the target-related information available during preparatory activity in the control
195 conditions (**Fig. 3c**). As in previous studies, we found that within the subspace spanned
196 by the first three principal components, preparatory activity was radially organized
197 according to the target-related reach direction (**Fig. 3d**) and trial time (captured by
198 PC3, **Fig. 3e**). A similar constellation was found when examining the control and HFS

199 data when the monkeys performed an 8-target reaching task (see Methods), where
200 we found both target-independent (**Fig. 3f,g**) and target-dependent (**Fig. 3h**) effects
201 of HFS on neural states compared to the control conditions. Specifically, the target-
202 dependent effects differentiate between distal targets located away from the body
203 (blue-shaded targets in **Fig. 3h**) and proximal targets located near the body (red-
204 shaded target) for which the effect of HFS was inverse.

205 **Preparatory activity was more sensitive to force field perturbation during the**
206 **cerebellar block**

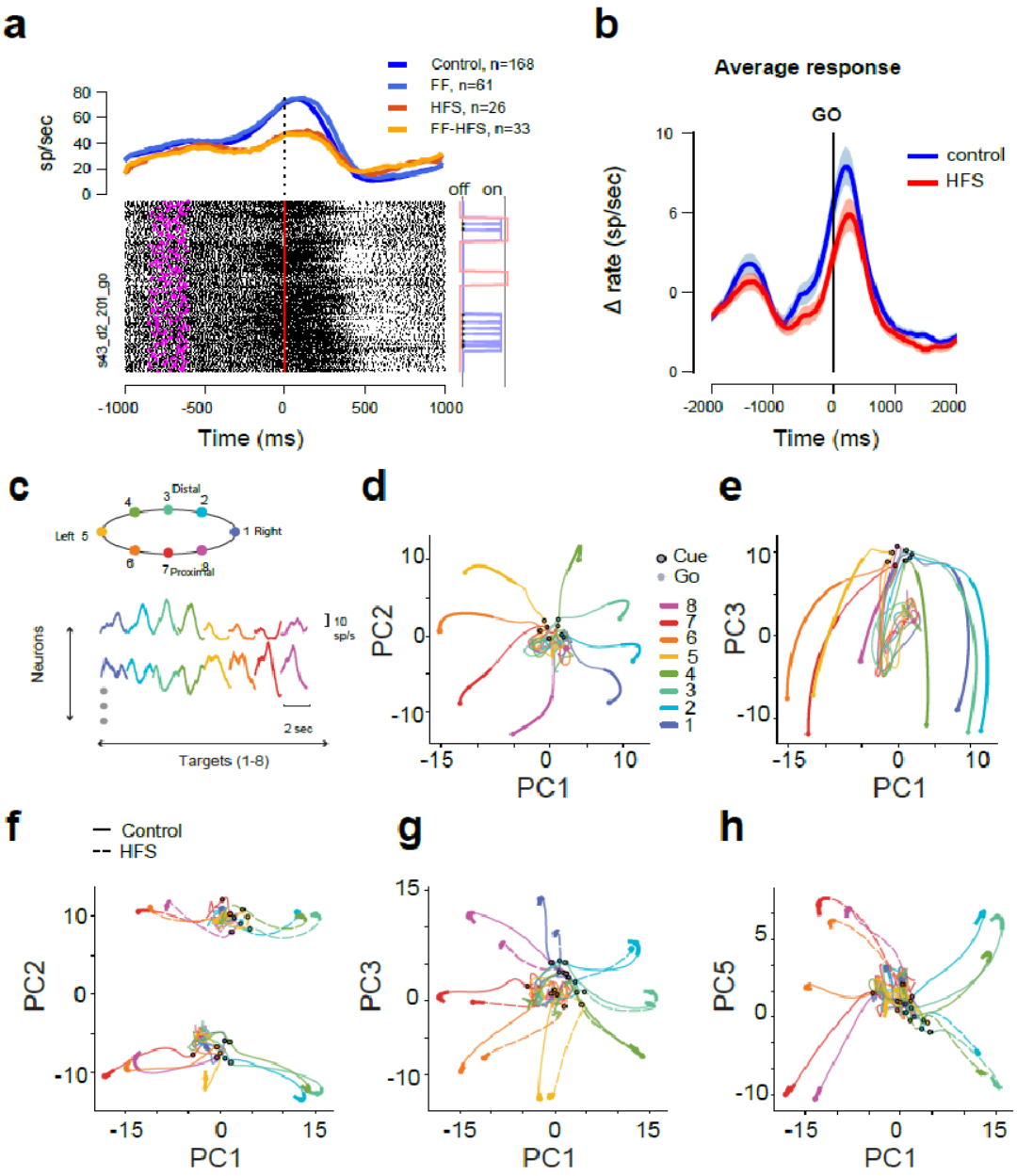

Figure 3. HFS alters neural activity in both a target-dependent and independent manner. a, An example of a motor cortical cell recorded during a single session. The figure only includes those trials in which movements were made towards the learned target (LT) in the four conditions (±HFS x ±FF). The bottom panel shows the raster plot, with trials aligned to the 'Go' signals (time 0), and magenta symbols denote cue onset times. The right-most panel shows the onset of FF (blue) and HFS (red) conditions during the session. Asterisks denote catch trials. Top: trial-averaged firing rate in the four conditions. b, Average task-related activity of all cells during the control and HFS conditions. Data from both monkeys were included (64 cells from monkey P and 154 cells from monkey S). Only cells that were directionally tuned ($p < 0.05$) during the Control-8 condition (control trials, each directed to 1 of 8 possible targets) and were recorded during all 4 test conditions (±HFS x ±FF) were considered. Single-cell PSTH was calculated around the 'Go' signal with a 50 ms bin size, and the resultant histogram was normalized by subtracting the pre-cue firing level. The shaded area around each curve depicts the standard error of the mean. c, Illustration of the target arrangement in the setup (indicating targets located distal/proximal/left/right relative to the monkey) and the way target-related population activity was calculated. For each cell, we concatenated the target-specific response (-1 sec to +1 sec around the 'Go' signal), forming a $n \times 8 \cdot t$ matrix, where n is the number of available neurons and $8 \cdot t$ is the total number of time bins spanning the response of each cell to the eight targets. The matrix was used for the PCA. d, Projection of single-cell activity on the first 2 PCs calculated as shown in panel c. Trajectories from trial onset to 'Go' signals are color-coded for the different targets. Colored symbols circled in black designate the 'Cue' signals, and filled circles designate 'Go' signals. Thick lines indicate the epoch used for calculating the PCA. e, Same as d but projecting on PC1 and PC3. f, To identify the impact of HFS on coordinated neural activity, we used a dataset in which neurons were recorded during the control and HFS conditions while the monkeys reached toward one of the eight different targets; see Methods). PCA was performed in a similar manner as in d and e, but with a data matrix of dimension *n x [8 x 2 x t]* where 2 corresponds to the control (solid lines) and HFS (dashed line) conditions. Activity was projected on PC1 and PC2. g, Same as panel f but projecting data on PC1 and PC3. h, Same as panel g but projecting data on PC1 and PC5.

During the adaptation trials, although the monkeys only experienced the force field when movement started, their pre-movement activity was considerably affected by the subsequent events. We analyzed the neural states for the four different conditions (±HFS, ±FF) during movement preparation and execution (**Fig. 4a,b** and **Supplemental Figure S1**). Since in any given learning session, all trials were directed towards a single target, we averaged the neural activity across targets to obtain the target-independent neural states. The effects of HFS and FF were clearly evident during movement when all four conditions were equally separable (**Fig. 4b**). Notably, however, the four conditions were already separable during movement preparation (**Fig. 4a**) but to varying extents, such that the separability between subsequent FF and null field (NF) trials was larger under HFS (red symbols) than in the control conditions (blue symbols). This property was quantified and verified by the decoding (FF vs. NF) accuracy (**Fig. 4c**), which showed that even though the noise level was the same in the two conditions, FF vs. NF decoding during the delay period was more accurate under HFS. Taken together, these results suggest that preparatory neural states encode the upcoming conditions of the trial (FF vs. NF), and that this sensitivity is accentuated during cerebellar block, although motor adaptation under these conditions was impaired.

225 **Changes in cortical activity within the target-related plane may drive residual**
226 **adaptation under HFS**

227 The augmented sensitivity of preparatory states to FF under HFS could underscore the
228 adaptation-related mechanisms employed in these conditions. We tested this
229 possibility by measuring changes in neural activity in the target-related subspace
230 correlated with the trial-to-trial adaptation to FF. We first applied targeted-
231 dimensionality reduction (TRD)[25,38] to the pre-learning trials, which identified the
232 plane in neural activity that best predicts the position of the targets (**Fig. 4d**). We then
233 projected the condition-specific (FF and FF-HFS) single-trial activity onto the plane
234 spanned by the first two dimensions of the TDR and measured its angular deviation
235 from the learned target. We found that during FF adaptation, the angular deviations
236 of single trials were centered around the learned targets, regardless of the FF direction
237 (clockwise or counterclockwise, **Fig. 4e**). Conversely, under FF-HFS, the single trial
238 angles had a substantially higher angular variance, with a significant rotation of the
239 mean bias consistent with the FF direction (**Fig. 4f,g**). Testing for a correlation
240 between the mean angular deviation and the adaptation process (**Fig. 4h** and
241 **Supplemental Figure S2)**) revealed how the gradual change in the angular deviation
242 as the error decreased. Specifically, during FF adaptation, when trajectory errors were
243 large (corresponding to early FF trials), neural activity only evidenced a small deviation
244 that continued to diminish throughout the adaptation process such that when the
245 errors were small (corresponding to late adaptation trials), the neural state was nearly
246 aligned with the learned target (**Fig. 4h**, blue lines). In stark contrast, under FF-HFS,
247 the angular settled when adaptation was completed at around 45 degrees (**Fig. 4h**,
248 red lines). Similar results were found when examining the correlations between the
249 neural angle and trial number along the adaptation session while ignoring the error
250 size in these trials (**Supplemental Figure S2**). This result suggests that the large
251 separation in trajectories between NF and FF conditions under HFS may at least
252 partially reflect an adaptive rotation of the neural angle away from the learned target.
253 The cortical change in neural angle may reflect a “re-aiming” policy used by the motor

system as a compensatory mechanism aimed to handle the force field in the absence of online cerebellar control.

Cerebellar signals induced task-relevant low-dimensional cortical representations

If the rotational shift in cortical preparatory states during FF-HFS represents a cortical compensatory mechanism, it could mean that cerebellar signals are not involved in shaping motor preparatory activity but function only as an online controller of movement. In this case, the preparatory state during null field conditions (when no cortical compensation is required since there is no adaptation) should not be affected by the HFS. To address this question and to quantify the effect of cerebellar signals on motor preparation, we calculated the effective dimensionality of cortical activity in the control and HFS conditions. To measure dimensionality, we calculated the

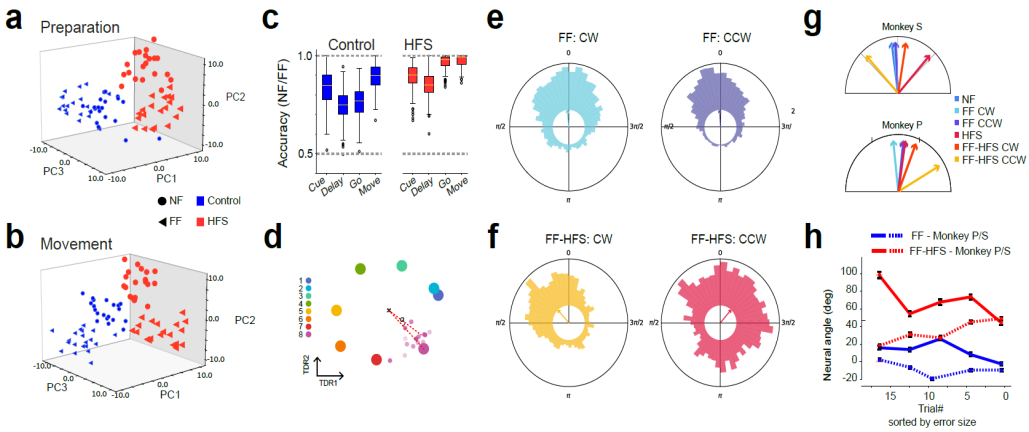

Figure 4. Preparatory neural activity during HFS is more sensitive to the subsequent force field. a, Projection of trial-specific coordinated activity on the first 3 PCs during preparation for movement. Each dot presents coordinated activity in a single trial during the sequence of trials performed in the control (blue) or HFS (red) conditions, either before adaptation (null field, NF - circles) or during adaptation (FF - circles). Neural data were averaged across all targets, and obtained during a time window spanning -300 ms to 0 around the Go signal. **b,** Same as **a** but calculated during the 100-400 ms after the Go signal. **c,** Decoding accuracy of adaptation conditions (NF vs. FF) based on epoch-specific data for the control (blue bars) or HFS (red bars). Dashed line denotes chance level (0.5). The different values for decoding accuracy were obtained for different realizations of the training and testing sets. **d,** Projection of target-specific neural activity 100 ms before the Go signal on the TDR axes. Large dots correspond to the trial-averaged activity used to compute the TDR axes, for each of the 8 targets. Small dots represent the activity in different trials associated with the 8th target in the Control condition. The neural angle denotes the angle of a trial's projection relative to the projection of the mean activity in the Control conditions for the same cued target. **e,** Polar histograms of the neural angles calculated for one monkey (monkey S) by aggregating data from all cued targets and trials in the control FF conditions with the same force field direction (left panel: clockwise CW trials, right panel: counter-clockwise CCW trials). **f,** Same as **e** but during FF combined with HFS (FF-HFS). **g,** Mean neural angles calculated for different force-field and HFS conditions, for monkey S (top panel) and P (bottom panel). **h,** Average neural angle as a function of trial number when sorted by trajectory errors (ordered from high to low maximal deviation). Neural angles for monkey P/S are shown respectively in full and dashed lines. Blue and red respectively indicate FF and FF-HFS conditions.

265 participation ratio[39,40] of the condition-average neural activity (see Methods) obtained
266 when the monkeys performed 8-direction reaching movements in the control and HFS
267 conditions. The a priori assumption is that the participation ratio should range from 2,
268 indicating that the trial-averaged activity of all the targets lie exactly on a single plane,
269 to 7, indicating that the neural representations of the eight targets are uncorrelated,
270 thus defining a 7-dimensional subspace. We found a significant increase in the
271 dimensionality of preparatory activity under HFS as compared to control conditions
272 (**Fig. 5a** and **Supplemental Figure S3**). In contrast, neural activity before the Cue and
273 after the Go events had a similar dimensionality (high and low, respectively) in the
274 control and HFS. This result is consistent with our previous report of decorrelated
275 activity during HFS[30].

276 To account for the ways in which cerebellar output modified the dimensionality of
277 motor cortical signals and the functional consequences of this effect, we implemented
278 a simple computational model of cerebellar-to-cortical interactions (**Fig. 5b)**. In this
279 model, the cortical network integrated two kinds of inputs: a high-dimensional target-
280 related command and low-dimensional cerebellar feedback. The low-dimensional
281 feedback is "task informed", since it conveys information about the spatial
282 arrangements of the learned targets relative to each other, which in our case
283 corresponds to a ring arrangement on a plane. Although there was no learning in the
284 modeled motor cortex and the cortical synapses were considered random, the low-
285 dimensional feedback was sufficient to quench motor cortical activity into an effective
286 lower-dimensional neural manifold, as measured by the participation ratio (i.e., Dpca).
287 Further, a reduction of the feedback gain resulted in an increase in dimensionality,
288 consistent with the increased dimensionality we found experimentally when blocking
289 cerebellar output (**Fig. 5c**).

290 **The increased dimensionality of cortical activity during HFS was accompanied by a**
291 **decrease in generalization performances**

292 The increased effective dimensionality during the preparation period suggests a loss
293 of structure in the neural representation and lower correlations between target-
294 specific neural representations. Previous studies have noted that low dimensional task
295 representations supported task abstraction, which is needed for generalization[41,42].
296 The ability to utilize an abstract representation for generalization can be measured by

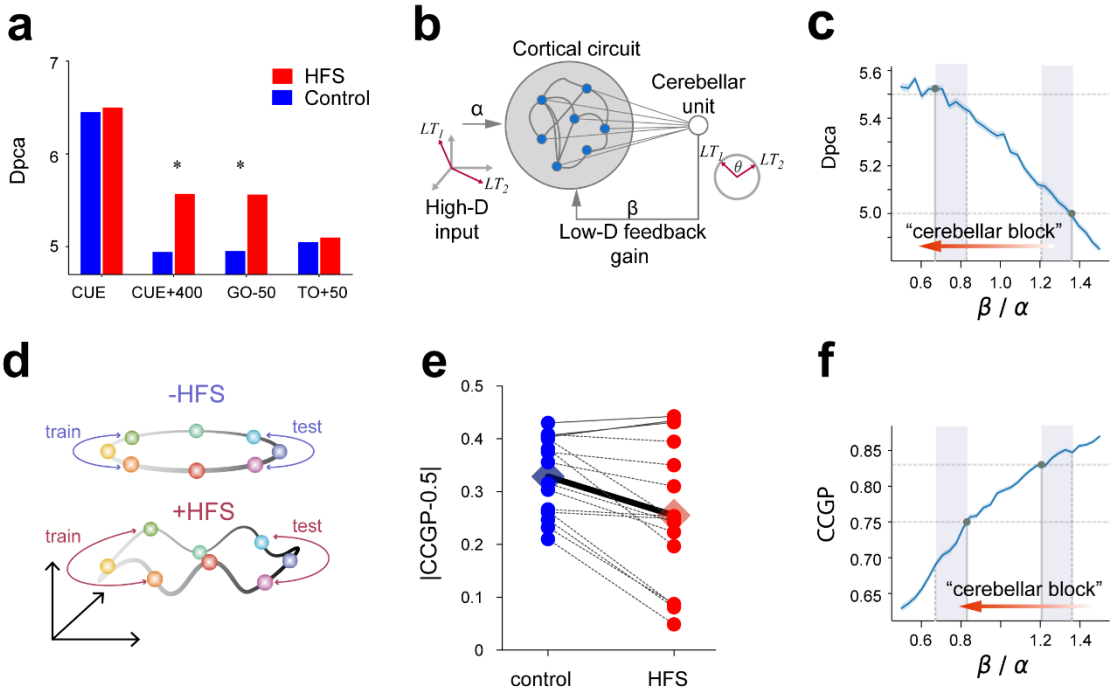

Figure 5. Cerebellar signals constrain the dimensionality of preparatory activity and improve generalization. **a,** Dimensionality of neural activity as estimated by the participation ratio (see Methods) at different time points during the control (blue) and HFS (red) conditions. The data were obtained from trials when monkeys performed 8-directional movements in the control or HFS conditions with no applied FF. Asterisks denote epochs with significant differences in dimensionality (Dpca) during the control vs. HFS conditions (1000 different network realizations, $p < 0.01$) **b,** A simple network model captures the effects of the low-dimensional cerebellar feedback on motor cortical activity. The recurrent network integrates the external high-dimensional command signal (with gain α) and the low-dimensional feedback (with gain β). At input, the targets are uncorrelated and are represented in the high-dimensional space. At feedback, the targets are embedded in a low-dimensional ring and are represented by a single variable θ. **c,** Dpca (participation ratio) calculated for the modeled cortical activity (as in b) is shown as a function of the low-dimensional feedback gain relative to the high-dimensional input (β/α). LT1 and LT2 are examples of different learned targets represented in the high-dimensional input and the low-dimensional cerebellar embedding. Horizontal dashed lines show the Dpca values obtained for the data in the control (lower level) and HFS (higher level). Solid vertical lines show the β/α value corresponding to the intersection point with the Dpca (marked in circles). Vertical dashed lines show the matching β/α values obtained when calculating CCGP (panel f below). The shaded area shows the low and high β/α -ranges that best fit the data with and without cerebellar block. The red arrow points to the gradient of β/α values that simulate the cerebellar block. The values used in this simulation were external gain α=0.25 and intercortical gain g = 1.75. The shaded area around the curve denotes the standard error over 600 different network realizations. **d,** Illustration depicting the effects of the topology of the neural representation on cross-condition generalization performance (CCGP). Increasing the dimensionality (e.g., the lower vs. the upper ring) impaired the performances of linear readouts trained on only half of the trials (e.g., the left side of the ring) when applied to unseen data (e.g., the right side). This simple heuristic explains the deterioration in CCGP (see Methods) on cortical activity under HFS compared to control conditions. **e,** CCGP relative to chance level (0.5) calculated for the Control (blue) or HFS (red) conditions. Each dot represents a different pair of dichotomies with shared symmetries (e.g., top-down dichotomy on left targets and top-down dichotomy on right targets). The diamonds represent the average CCGP over all pairs of dichotomies. **f,** Similar to c but for the CCGP computed for the network model depicted in b as a function of the low-dimensional feedback gain.

297 the Cross-Condition Generalization Performance (CCGP) of a linear readout[41]. To
298 demonstrate how dimensionality and structure enable generalization, one can
299 consider a dataset generated from a ring embedded in a high-dimensional space. After
300 dividing the ring into four quadrants, it is possible to train a linear classifier to separate
301 data taken from top and bottom halves of the circle on the left side and test its
302 performances on data taken from the right side of the ring. If the ring is perfectly
303 embedded within a two-dimensional subspace, the effective dimensionality is d=2,
304 and the classification would generalize well. On the other hand, if the ring is
305 embedded through a nonlinear transformation and does not lie within a single plane,
306 the effective dimension would increase, and the generalization performance would
307 diminish[41] (**Fig. 5d**). Thus, the CCGP can measure the generalization performance

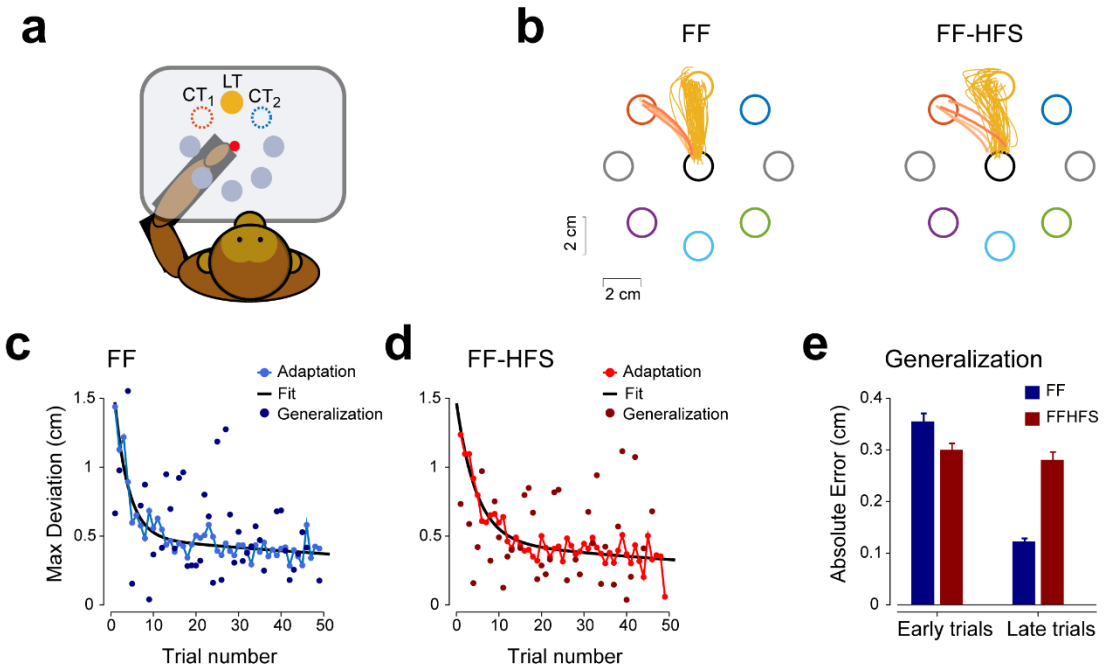

Figure 6. Impaired generalization behavior during HFS trials. a, Monkeys performed the same task as shown in Figure 1a. However, during the adaptation sequences, we used randomly selected probe trials in which the monkeys were instructed to move to one of two targets, flanking the learned target. This approach was used to estimate the generalization of learned behavior to nearby targets. **b,** Example of one session in which probe trials were presented to the left of the learned target during FF (left panel) and FF-HFS (right panel) conditions. The hue of the probe trajectories indicates the order of trial presentation in the sequence (light/dark - early to late trials, respectively). **c,** Summary of adaptation and generalization across all sessions. The adaptation sequence (light blue lines and symbols) and a fitted adaptation curve (dark blue) are shown. The generalization samples show the (non-averaged) deviation in all probe trials presented at different positions during the adaptation session. **d,** Same as panel i but for the FF-HFS conditions. **e,** Quantification of generalization across all sessions, calculated for early (1-5) and late (>= 10) trials in the FF (blue) and HFS (red) conditions.

308 across different possible dichotomies of the ring. Following this argument, we
309 quantified the task abstraction in the cortical representations by calculating the CCGP

310 during the preparatory period. As expected, the increased dimensionality in the
311 presence of HFS was accompanied by a decrease in the CCGP (**Fig. 5e**). This result was
312 also replicated in our simplified model where the decrease in the low-dimensional
313 feedback resulted in increased dimensionality and decreased CCPG (**Fig. 5f**).

314 Finally, we tested whether the increased dimensionality and reduced generalizability
315 of task-related neural activity under HFS would also extend to changes in behavior. To
316 this end, we tested the ability to generalize learned behavior to untested targets
317 under HFS. Specifically, a monkey was required to implement an adapted response
318 acquired from the learned target to movements directed to neighboring targets (**Fig.**
319 **6a,b**). We found that blocking cerebellar output using HFS impaired the ability to
320 generalize target-specific adapted behavior. The effect of HFS was specifically
321 pronounced when generalization trials presented late on the adaptation block when
322 adaptation to the learned target was completed (2-way Repeated Measures ANOVA,
323 stimulation × time interaction, p=7.4e-3). Late, but not early, generalization was
324 significantly impaired compared to the control condition (t-test p=0.022) (**Fig. 6c-k**).
325 These results are aligned with previous models, suggesting that the cerebellum
326 encodes task-specific information[43]. Taken together, these results suggest that
327 cerebellar signals may play a dual role in regulating FF adaptation and generalization
328 through their specific roles in motor execution and motor preparation.

329

330 ## Discussion

331 The cerebellum plays a key role in motor adaptation[1,2,44], but neural correlates of
332 adaptive responses can also be found in the motor cortex as early as the preparatory
333 period [22,25,34]. These early cortical signals may be an outcome of cerebellar-to-cortical
334 interactions[27-29] or evolve locally through intracortical processes. Here we addressed
335 this question by reversibly blocking cerebellar outflow while monkeys performed a
336 force-field adaptation task. We found that this manipulation led to increased motor
337 noise and impaired adaptation that were accompanied by two notable changes in the
338 preparatory neural state. First, in FF-HFS, neural trajectories calculated before

339 movement onset shifted away from the learned target, whereas during FF trials, the
340 neural trajectories remained aligned. Second, under HFS, the dimensionality of
341 preparatory activity increased, leading to a more complex and less generalizable
342 neural space. This outcome was explained by a computational model that showed that
343 a low-dimensional cerebellar-like input can lead to a cortical network with reduced
344 dimensionality. In addition, the model predicted that the loss of cerebellar signals
345 would lead to impaired generalization, as confirmed experimentally in the reduced
346 generalization under HFS at both the neural and behavioral levels.

347 These adaptation-related motor impairments under HFS closely resemble the deficits
348 found in cerebellar patients. The adaptation to the force field under HFS was impaired
349 (**Fig. 1d, g**) but not completely abolished. Similarly, adaptation in cerebellar patients
350 to a repeatedly presented target was shown to be maintained even in severely
351 affected subjects[31,45-47]. In addition, the poor adaptation during HFS was driven by low
352 error sensitivity (**Fig. 2a**), reflecting the lesser capacity of the system to learn from
353 previous errors[37], and increased motor noise as measured by the trial-to-trial
354 variability of hand trajectories (**Fig. 1c**). Augmented motor variability is a core
355 symptom in cerebellar patients [15,45,48-51], although it was shown that motor noise alone
356 is insufficient to explain the reduced error sensitivity and the subsequent impaired
357 adaptation [32]. Likewise, the low error sensitivity under HFS was maintained even when
358 matching the error size to the control conditions (**Fig 2d**), thus indicating that without
359 cerebellar signals, the ability to learn from previous errors is fundamentally disrupted.
360 Taken together, these results show that HFS accurately replicated both the difficulties
361 exhibited by cerebellar patients when trying to adapt to an external force field [48,52,53]
362 and the underlying mechanisms leading to these impairments.

363 Blocking cerebellar signals during motor adaptation trials led to a significant alteration
364 in pre-movement motor cortical activity. The preparatory neural state under HFS was
365 more sensitive to the subsequent force field compared to the control conditions (**Fig.
366 4a-c**), which may hint at more adequate preparation for the upcoming perturbation
367 despite the impaired adaptive behavior in this condition. In addition, during FF-HFS
368 trials (but not in FF trials) the neural angle of the preparatory state (calculated in the

369 target-related subspace) rotated in a way that was correlated with the direction of the
370 subsequent force field (**Fig. 4g)**. By the end of the adaptation, the neural angle
371 hovered around 45° relative to the learned target in what could be interpreted as a
372 re-aiming strategy (**Fig. 4h)**. Studies on cerebellar patients have also revealed
373 asymmetries in adaptation between CW and CCW. It is argued that these patients
374 manage to compensate for the loss of cerebellar predictive signals by using a volitional
375 (cortically-based) strategy to leverage the directional force field to complete the
376 task[31]. Our results are fully consistent with this hypothesis. Hence, in the absence of
377 cerebellar signals, the motor cortex appears to be able to identify patterns in the
378 external environment and adjust its motor plan to suit (or leverage) these patterns in
379 an effort to reduce error. This result departs from other reports[25], which found a re-
380 aiming strategy during FF adaptation. This outcome could be related to the differences
381 in task conditions since Sun et al. used a haptic device and isometric wrist movements,
382 which resulted in slower adaptation. Importantly, our findings show that adaptation
383 to FF does not require a rotational shift in cortical activity as long as the cortico-
384 cerebellar circuit is intact.

385 The involvement of cerebellar signals in shaping preparatory activity may extend
386 beyond motor adaptation tasks. Previous studies have reported that the cerebellum
387 is involved in the planning stage of motor control[27,28,54]. The current findings support
388 and add to these data by showing that cerebellar signals shape cortical preparatory
389 activity by providing task-relevant information. Our analysis of the preparatory neural
390 trajectories in the null field conditions revealed that part of the effect of HFS was
391 target-dependent, and involved distinguishing between distal and proximal targets
392 (**Fig. 3h**), suggesting that this information is embedded in the cerebellar output
393 normally converging onto the motor cortical network. In addition, we showed that
394 cerebellar signals participate in regulating the dimensionality of preparatory activity,
395 such that in their absence, this dimensionality increases significantly (**Fig. 5a**). This
396 outcome suggests that the cerebellum is responsible, at least in part, for the
397 embedding of motor cortical activity within a low-dimensional manifold[55-57]. The
398 cerebellum can achieve this by learning the structure of the task and projecting it back

399 to the cortex via the thalamus[43]. Consistent with this hypothesis, our computational
400 model showed that recurrent feedback that learned the structure of a task was
401 sufficient to reduce the cortical dimensionality, whereas decreasing the gain of this
402 feedback led to an increase in dimensionality as it occurred under HFS (**Fig. 5c**).

403 Our neural analysis and behavioral results further suggest that the dimensionality
404 reduction of cortical activity to a low-dimensional manifold can affect motor
405 adaptation. Under HFS, the increased dimensionality of the target-related manifold
406 implies a topological change in the neural representation that disrupts the geometric
407 relations (angles) between the targets in the neural space. In particular, the
408 topological change impedes task abstraction, as measured by the decrease in the
409 Cross-Condition Generalization Performance (CCGP) under HFS (**Fig. 5e**). The CCGP
410 measures how well a linear readout trained on part of the manifold can generalize to
411 unexplored regions of the manifold[41]. Our computational model confirmed this result
412 by showing that decreasing the gain of the low-dimensional feedback to the cortical
413 circuit not only increased the dimensionality, but also resulted in a lower CCGP (**Fig.
414 5f**). Although CCGP directly measures generalization performance in a linear
415 classification, it may also account for impairments in generalizing adapted responses.
416 This is because generalization of both classification and adaptation relies on
417 symmetries in the neural representations that are broken when the dimensionality
418 increases. In accordance with our neural observations, our behavioral analysis showed
419 that during the cerebellar block, monkeys failed to generalize to neighboring targets,
420 similar to previous studies showing impaired generalization in cerebellar patients [31,58].
421 One limitation of this approach is that our analysis of neural states cannot directly
422 account for the observation that in a motor adaptation task, the ability to generalize
423 decreases as the angle from the learned target increases[8,25,59,60]. It is possible that
424 since the dimensionality of the preparatory state was already high in the control
425 conditions ($D_{PCA} > 5$) the targets did not reside perfectly in a single plane and that
426 this baseline topology of population activity impeded generalization to distant targets
427 even when no HFS was applied.

428 Finally, our results propose a new way to link between motor adaptation and
429 generalization. It is possible that under HFS, when the dimensionality of activity
430 increases and the task structure is impaired, adaptation can only be local, since the
431 specific adjustments required for adapting to target-specific force fields are
432 uncorrelated across targets. In this model, the preparatory rotation of the cortical
433 state constitutes the implementation of this local learning. The rich set of
434 sensorimotor inputs integrated by the cerebellum from via mossy fibers[61], as well as
435 task-related representations such as error and reward signals from climbing fiber
436 inputs[10,62] place the cerebellum in an ideal position for structuring the cortical
437 representation and facilitating the embedding of the complex external world into an
438 egocentric cortical representation, in a process akin to coordinate transformation[63]. A
439 future combination of experimental and computational studies is needed to validate
440 this hypothesis.

441

442 **Methods**

443 **Behavioral paradigms**

444 Data were obtained from 5 *Macaca Fascicularis* monkeys (females, 4.5-5.5 Kg).
445 Monkey care and surgical procedures were in accordance with the Hebrew University
446 Guidelines for the Use and Care of Laboratory Animals in Research, supervised by the
447 Institutional Committee for Animal Care and Use.

448 Force field adaptation task. Two monkeys were trained to sit in a primate chair, wear
449 an exoskeleton (KINARM, BKIN technologies) and perform a planar, shoulder-elbow
450 reaching task (**Fig. 1a**). In this task, the monkeys were instructed to locate a cursor
451 within a central target. After 500 (monkey P) or 800 (monkey S) msec (pre cue period),
452 a peripheral target (one of 8 evenly distributed targets) appeared and the monkey had
453 to wait another 600-850 (monkey P) or 450-700 (monkey S) msec (delay period) until
454 the central target disappeared ("go" signal) and reach the cued peripheral targets
455 within 800 (monkey P) or 900 (monkey S) msec. If the monkey moved the cursor to
456 the correct target within this time frame it was rewarded with a drop of applesauce.

457 Eight-target task. Monkey P and two additional monkeys (monkeys C and M) were
458 trained to perform an 8- target reaching task in the control and HFS conditions. This
459 task is described in detail in [30,64,65]. In short, the monkeys were instructed to locate a
460 cursor within a central target. After 500 ms, a peripheral target appeared and the
461 monkey had to wait until the central target disappeared (''GO'' signal) and then reach
462 the cued peripheral targets. If the monkey moved the cursor to the correct target
463 within the predefined time limit, it was rewarded with a drop of applesauce. To
464 encourage the monkey to predict the timing of the ''go'' signal, we limited the total
465 time it had to reach the peripheral target to 500 ms and inserted a 200 ms grace period
466 before the GO signal. Onset of movement within this time frame did not abort the
467 trial.

468 **Surgical procedure**

469 After training was completed, in a surgical procedure under general anesthesia, a
470 recording chamber (21x21 mm) was attached to the monkeys' skull above the hand-
471 related area of the motor cortex and a small chamber was positioned above the
472 estimated insertion point of a stimulating electrode at the Superior Cerebellar
473 Peduncle (SCP). After recovery and a re-training period, we recorded motor cortical
474 activity extracellularly. During recording sessions, glass coated tungsten electrodes
475 (impedance 300-800 kU at 1,000 Hz) were lowered through the chamber to different
476 cortical sites, mostly in the primary motor cortex (M1). The signal obtained from each
477 electrode was amplified (x10K), and bandpass-filtered online (300-6,000 Hz). The
478 signal was then digitized (32 kHz) and saved to disk.

479 **Insertion of stimulating electrode into the SCP**

480 A post-surgery MRI scan was used to plan the insertion trajectory of the stimulating
481 electrode into the ipsilateral SCP through the small chamber. Then, we inserted a
482 chronic bi-polar stimulation electrode into the SCP (NSEX100, David Kopf Instruments,
483 impedance range of 30-60 KΩ). To verify the correct placement of the implanted
484 electrode, we applied bipolar stimulation pulses through the electrode and monitored

485 the evoked intra-cortical responses measured by recording electrodes inserted in the
486 motor cortex [66,67].

487 **Experimental protocols**

488 Force-field adaptation protocol. Each recording session was composed of two or three
489 sub-sessions, with each session spanning 340 trials that followed a similar protocol.
490 Each sub-session included a set of control trials directed towards all 8 target
491 directions. Afterwards, one of the 8 possible targets was selected as the Learned
492 Target (LT) and all the trials thereafter were directed towards this target. These trials
493 included a set of control trials (with no force-field and/or HFS), a set of trials with HFS,
494 force field trials (FF) and force field trials with HFS (FF-HFS). Each condition was
495 separated by washout trials which were also directed towards the learned target but
496 with no FF or HFS applied. These trial sets were inserted between FF and HFS sets and
497 between HFS and FF-HFS sets. During the adaptation sequence we inserted
498 intermittent catch trials in which the force field was unexpectedly removed. Catch
499 trials appeared at random in about 10% of the trials

500 Generalization protocol. In one monkey (monkey P) we tested its ability to generalize
501 the force field learned for the LT to movements directed to neighboring targets. In
502 these experiments we used only the most distal and most proximal targets in the
503 anterior-posterior axis (target 3 and 7 in **Fig. 1a**) as the learned targets. In each sub-
504 session we selected one learned target and one of its neighboring targets (either to its
505 left or right) as the probe target. During the adaptation set, we randomly inserted
506 probe trials (on average, every 10 trials) in which the probe target was presented
507 instead of the LT. The direction of the applied FF was randomly selected to be either
508 CW or CCW.

509 **Electrophysiological recordings**

510 Glass coated tungsten electrodes (impedance 300-800 kΩ at 1,000 Hz) were inserted
511 through the chamber to different cortical sites, mostly in M1. The signal obtained from
512 each electrode was amplified ($x10^4$), bandpass-filtered (300-6,000 Hz), digitized (32

513 kHz), and saved to disk. Recordings were made with up to 4 individually moveable
514 electrodes (Flex-MT by Alpha Omega, Nazareth, Israel).

515 We used the raw neural signal and first removed the stimulation artifacts by
516 subtracting their average profiles[66,67]. Then, we offline-sorted the cleaned signal to
517 extract spikes of single cells (Offline Sorter™, PLEXON). Cell activity was further
518 inspected to confirm stable trial-to-trial activity during recordings.

519 **SCP stimulation protocol**

520 To block the outflow of cerebellar signals, we applied high-frequency stimulation (HFS)
521 through a chronic SCP stimulating electrode [Nashef et al. 2019]. HFS consisted of a
522 long train of biphasic (200 µs each phase) stimulation pulses applied at 130 Hz, and
523 delivered at fixed intensity (ranging from 75 to 200 µA). The HFS trains were applied
524 during a sequence of 30-50 trials either in combination with the force field (FF-HFS
525 trials) or in the null-field conditions (HFS trials).

526 **Analyses of motor behavior**

527 Behavioral analysis of the force-field adaptation process. During task performance the
528 KINARM system (BKIN Technologies, Canada) provided continuous measures of the
529 angular velocities of the shoulder and elbow joints and the endpoint position of the
530 working arm. We used these measures to compute the maximal velocity, movement
531 time, curvature index, and reaction time for each trial.

532 During the force field adaptation trials, the motors of the exoskeleton generated a
533 velocity-dependent curl field orthogonal to the direction of the hand velocity in a
534 clockwise or counter-clockwise direction, according to:

535 (1) $$\begin{bmatrix} F_X \\ F_Y \end{bmatrix} = k \begin{bmatrix} \cos(\theta) & -\sin(\theta) \\ \sin(\theta) & \cos(\theta) \end{bmatrix} \begin{bmatrix} \dot{X} \\ \dot{Y} \end{bmatrix},$$

536

537 where F_x and F_y are the forces generated by the robot in x and y axes, respectively,
538 k=3 Ns/mm, $\theta = \pm\frac{\pi}{2}$, and $[\dot{x}, \dot{y}]$ is the hand velocity vector in the horizontal plane.

When applied, the curl force field changed the arm dynamics and caused a deflection of the movements from the straight trajectory line.

Measuring the adaptation process. For each trial n we calculated the motor response $r^{(n)}$, which we defined as the maximal deviation of the trajectory from a straight line connecting the initiation and end point. We also measured the deviation at an early time point (150 ms after movement onset). To compare the adaptation curves between control and HFS trials, for which movement velocity varied, single session data were normalized by dividing the trial-specific trajectory errors by the error measured for the first trial. This forced all single session adaptation curves to start at 1. To analyze the differences between adaptation during FF and FF-HFS, we divided the deviation data into four bins of 10 trials each and applied two-way ANOVAs with HFS (+/-) as one factor and adaptation bin as the second factor.

Calculating the Learning Index. To quantify the accumulating effect of adaptation, we calculated the *Learning Index* (LI)[33]. First, we calculated the net response by discounting the natural tendency of the monkey to produce stereotyped movement $\delta r^{(n)} = r^{(n)} - < r >$, where $< r >$ denotes averaging th(e response over 20 control trials to the learned target, performed immediately before the adaptation set. The *Learning Index* at catch trial n is the absolute net response relative to the response in flanking trials

$$(2)\ Learning\ Index(n) = \frac{|\delta r^{(n)}{}_{catch}|}{|\delta r^{(n)}{}_{catch}| + |\delta r^{(n)}{}_{field}|}$$

where $\delta r^{(n)}{}_{field} = (\delta r^{(n-1)} + \delta r^{(n+1)})/2$. During normal adaptation, δr_{field} decreased in size while δr_{catch} increased leading to an increase in the learning index. *Learning Indices* were ordered according to their location in the adaptation sequence (i.e., the sequential numbers of the catch trials), and then averaged to yield the mean learning index curve as a function of trial number.

Measuring the within-session adaptation process. To verify that learning converged not only on average, but also in individual sessions, we correlated the motor error (hand deviation) with the trial number. The underlying assumption was that in a case

of a monotonic decrease in error along the adaptation session the correlation coefficient should obtain a negative value. On the other hand, low (near-zero) correlation values will correspond to variable adaptation processes with a high trial-to-trial error variability.

Calculating the error sensitivity and retention factor. We used a simple linear state-space model (SSM)[37] to model behavioral adaptation across trials. We assumed that the motor response at trial n, which we denote by $r^{(n)}$ followed a simple linear evolution given by

(3) $r^{(n)} = ar^{(n-1)} + b^{(n)}e^{(n-1)} + \xi^{(n)}$.

where a is the retention factor, which measures the exponential decay in the internal state in the absence of error signal, $b^{(n)}$ is the error sensitivity, which could potentially change from trial to trial, and $e^{(n)}$ is the error on that trial. The noise term $\xi^{(n)}$ is a random Gaussian variable denoting trial-to-trial noise.

The error in each trial was expressed as the difference between the external perturbation, $\delta^{(n)}$ and the motor output $e^{(n)} = \delta^{(n)} - r^{(n)}$. In our setting, all perturbations were uniform in size, so we scaled the parameters accordingly and defined

(4) $e^{(n)} = 1 - r^{(n)}$

We used the SSM to calculate the retention factor a and the error sensitivity $b^{(n)}$ from our data. The retention factor was defined as the exponential decay of the motor behavior in the absence of error feedback and perturbations. For that purpose, we used washout trials, and calculated the average decay rate as

(5) $a = E\left[\frac{1}{P}\sum_{m}^{P}\left(\frac{r^{(m)}}{r^{(1)}}\right)^{\frac{1}{m-1}}\right]$,

where m is the trial index in the washout period with a total of P washout trials, and the expectation, $E[\cdot]$, denotes averaging across all sessions. Note that there was no significant difference in the retention factor across sessions.

Using the retention factor, we calculated the average error sensitivity in each session in the following manner:

(6) $b = \frac{1}{N}\sum_{n}^{N}\frac{r^{(n+1)}-ar^{(n)}}{e^{(n)}}$,

Where n is the trial index. Note that the effects of the noise $\xi^{(n)}$ were neglected since the trials were averaged. To compare the effect of HFS on error sensitivity we used the mean error sensitivity across adaptation trials.

<u>Motor noise and adaptive response</u>. Motor noise was defined as the mean of the absolute deviations (MAD) across all trajectory errors (measured at maximal deviation) during a set of trials. In each sub-session, noise levels were calculated separately for the control and HFS trials. To match the levels of noise between the control and HFS conditions we used the ratio of the calculated noise values between these conditions and considered those sessions in which the ratio ranged from 0.6 to 1.4 as matched.

To identify the type of motor noise in each condition we calculated the difference between the adaptive response in trial n, denoted by $R^{(n)}$,to the external noise. As in previous studies, we defined the adaptive response as the difference between the preceding and the subsequent errors:

(7) $R^{(n)} = e^{(n+1)} - e^{(n-1)} = r^{(n-1)} - r^{(n+1)}$

<u>Quantifying generalization behavior.</u> For each of the probe targets (located ±45° from the learned target) and each generalization trial, we first calculated the maximal deviation of the trajectory from the shortest (straight) line connecting the start and end points (generalization points in Fig. 5 i,j). Next, we calculated the absolute error (i.e., distance) between these deviations and a two-exponential model (in the form of $\boldsymbol{f(n) = a_1 e^{-b_1 \cdot n} + a_2 \cdot e^{-b_2 \cdot n}}$) best fitted (i.e., minimizing the mean-squared error) to the average adaptation curve calculated across all generalization sessions (solid lines in Fig. 5i,j). To assess the generalization performances along the adaptation session we defined early (trials 1-5) and late (trial number 10th and above) phases of adaptation.

621 **Neural data analysis**

622 To analyze adaptation, we collected a total of 514 cells from monkey P and 366 cells
623 from monkey S. In addition, to compare the effect of HFS on the 8-target reaching
624 task, we collected 355 cells from monkey C, 239 cells from monkey M and 183 cells
625 from monkey P (on top of the 514 cells used for studying FF adaptation). Different
626 analyses required different selection criteria and thus used different numbers of cells.

627 Pre-processing of the neuronal data. We selected neurons recorded in at least
628 *tr_tresh* trials in each of the four task conditions (see Table I for the exact value of
629 *tr_tresh* set for the different analyses). For the selected neurons, spike trains were
630 convolved with a Gaussian kernel of σ ms (Table I). Next, we averaged over trials with
631 similar conditions and formed an order-3 tensor [neurons x conditions x time], which
632 we denoted X. Finally, we selected a specific *time window* and z-scored the data over
633 both the condition and time dimensions,

634 (8) $X_{z-scored} = \frac{X - <X>_{conditions,time\ window}}{std_{conditions,time\ window}(X)}$.

635 We ran a PCA on the z-scored data by first concatenating conditions and time
636 windows, to generate a matrix calculated on *tr_tresh* with dimensions neurons x
637 [conditions x time_window].

	Conditions	tr_thresh	**σ**(ms)	time window (ms)
Fig.3 d,e	8 (eight targets)	1	100	[-300;0] r.t. GO
Fig.3 f,g,h	16 (eight targets/±HFS)	1	100	[-100;+50] r.t. GO
Fig.4 a	4 (±FF/±HFS)	10	100	[-300;0] r.t. GO (left panel) and [100;400] r.t. GO (right panel)
Fig.4 b	4 (±FF/±HFS)	10	50	[-500;-400], [-300;-200], [-50;50] and [200,300] r.t. GO
Fig.4 d,e,f	8 (eight targets)	1	100	10 ms
Fig.5 b	8 (eight targets)	1*	100	from left to right, [0;5] r.t. CUE; [400;405] r.t. CUE; [-50;-45] r.t. GO; [50;55] r.t. MO
Fig.5 c	8 (eight targets)	1**	100	[-200;0] r.t. GO

Table I. Selected parameters used for each analysis and corresponding figures.

*Trial selection is described below in PCA dimensionality.

**The trial selection criteria for the CCGP analysis are described in the Cross Condition Generalization Performance (CCGP) section below.

PCA dimensionality. To estimate the dimensionality of the neural representation, we calculated the participation dimension of the mean activity pattern across all targets. We first selected neurons with more than 40 trials across all targets under HFS (in addition to the *tr_thresh* condition on trials per target as described above). We then averaged the trials for each condition, resulting in eight mean vectors for each ±HFS. For the two conditions, we computed the correlation matrix across the 8 targets, and calculated the participation dimension,

(9) $$D_{PCA} = \frac{(\sum_n \lambda_n)^2}{(\sum_n \lambda_n^2)}$$

Here, λ_n for $n = 1, \ldots, 8$ stand for the eigenvalues of the correlation matrix targets. averaged across all trials for a specific condition. Note that we subsampled trials after grouping the different targets so that both the Control and HFS data tensors would have the same number of trials for a given target, and averaged across different trial

654 sections. As a result, the variance for control was higher due to the greater number of
655 trials.

656 Null Field/FF classification accuracy. The data were preprocessed with parameters
657 **tr_thresh**=10, **σ**=50 ms, **time window**=100 ms and the four task conditions
658 (±FF/±HFS). Individual trials were projected onto the first 15 PCs and a test set was
659 constructed by taking half of the total number of trials. A linear classifier was trained
660 using the LinearSVC library on the training set composed of the remaining trials to
661 discriminate between Null Field and Force Field under both Control and HFS
662 conditions. We computed the classifying accuracy for 10000 samples of test and train
663 sets (**Fig. 4c**) by taking the rate of correct classifications over both the number of test
664 trials for a given sample and the time window.

665 Targeted dimensionality reduction (TDR). We applied a targeted dimensionality
666 reduction analysis[38] to our dataset to associate variations in neural activity to the
667 position of the cued target. We first preprocessed the data (see above) using the
668 following parameters: *tr_thresh*=1, *σ*=100 ms and *time window*=10 ms. We then
669 expressed the z-scored responses of neuron i at time t to target k (where $k = 1, \ldots, 8$
670 is the target index) denoted by ${s^k}_{i,t}$ as a linear combination of task variables; i.e., the
671 x and y positions of the eight cued targets:

672 (10) $$r_{i,t}(k) = {\beta^1}_{i,t} {x^{(k)}}_{position} + {\beta^2}_{i,t} {y^{(k)}}_{position} + {\beta^3}_{i,t}.$$

673 We then selected the times ${t^{1,2,3}}_{max}$ at which ${\beta^{1,2,3}}_{i,t_{max}}$ had a maximal norm over
674 the given time window. Then, we orthogonalized the set of vectors $\beta^{1,2,3}_{t_{max}}$ with the QR-
675 decomposition to derive a set of three TDR axes; the first two define a plane that best
676 explained the x and y positions of the cued target and the third was a fixed bias axis.

677 Neural angle analysis. To calculate the neural angle, we only considered neurons with
678 minimal numbers of trials (-FF: 15 trials for monkey S and 10 for monkey P; +FF: 25
679 trials). Next, we computed the target-related TDR axes using the neural data for the
680 eight targets under the control conditions. We trial averaged the neural activity for
681 different HFS/FF conditions, and projected them on the target plane found using the

682 TDR analysis. The points resulting from the projections of the neural states were
683 parameterized in polar coordinates by their radius and angle (r,θ). Thus, the angle θ
684 obtained during movement preparation predicted the chosen target while the radius
685 r indicated the strength of this prediction. We eliminated projections that fell below a
686 threshold radius ratio **rr** calculated as a neural state's radius to the average radius of
687 the neural states used for computing the TDR axes,

688 (11) $$rr = \frac{r}{<r_{control8}>} > 0.5$$

689 The selected angles corresponding to 10 ms time windows in the range of -500 to -150
690 ms around the GO signal for monkey S (-200 to 0 around the GO for monkey P) were
691 aggregated to generate angular histograms.

692 Cross-condition generalization performance (CCGP). We evaluated the cross-
693 condition generalization performance (CCGP) of the target-related neural manifold, as
694 described by[41] separately in -HFS/-FF and +HFS/-FF conditions. We first selected
695 neurons with more than 40 trials, all targets considered, in the -HFS/-FF and +HFS/-FF
696 conditions. Next, we selected trials to ensure an equal number of trials for all
697 neuron/target combinations between -HFS/-FF and +HFS/-FF. Then, we applied the
698 preprocessing procedure with the parameters specified in the table, and created 1000
699 neural trajectories by random trial index shuffling for all neuron/target combinations.
700 Finally, we analyzed the 36 pairs of dichotomies available for the targets positioned in
701 a rectangle. For each pair, we determined the hyperplane for the first dichotomy and
702 assessed the performance of this hyperplane on the other dichotomy (using the
703 LinearSVC library). For example, we trained a linear decoder to discriminate between
704 neural activity associated with a top-left and a top-right target, and then tested this
705 decoder on neural activity associated with bottom-left and bottom-right targets. For
706 presentation purposes, we only used dichotomies with CCGP>0.7 under the -HFS/-FF
707 condition (where CCGP = 0.5 is the chance level).

708 **Computational model**

709 To study the capacity of cerebellar input to reduce cortical dimensionality and improve
710 the generalization of the linear readout we implemented a computational model of

711 cerebellar-to-cortical interactions. The model consisted of a simple recurrent cortical
712 layer and a low-dimensional feedback loop[68,69] where the cortex receives an external
713 command indicating which out of the eight possible targets was selected. Importantly,
714 the command was unstructured and did not contain any topological relations between
715 targets. The cerebellar feedback was trained to read out the cortical activity and
716 return the coordinates of the selected target on a 2- dimensional plane (structured
717 input).

718 The dynamics of the cortical neurons are given by the circuit equations[70]:

719 (12) $$\tau \frac{d}{dt} x(t) = -x(t) + \frac{g}{\sqrt{N}} W^{ctx}\ r(t) + \alpha W^{ex} u^0 + \beta W^{crb} z(t).$$

720 where $x(t)$ is a N-dimensional vector representing the membrane potential of the
721 cortical neurons. The instantaneous firing rate of each neuron i is given by $r_i(t) =$
722 $tanh\ x_i(t)$. The dense cortical recurrent connectivity is given by the N-by- N matrix
723 W^{ctx}, whose entries are sampled, *i.i.d.* from a standard distribution (a normal
724 distribution with zero mean and unit variance). The parameter g measures the
725 disorder in the system and provides the network with cortex-like activity [Sompolinsky
726 et al., 1988, Kadmon and Sompolinsky, 2015]. The 8-dimensional vector u^0 is a 1-hot
727 encoded vector representing the target identity: for each target, one component of
728 u^0 is '*1*' while the rest are '*0*'. The external input is fed into the network through the
729 N-by-*8* matrix W^{crb}, whose entries are sampled *i.i.d.* from a standard distribution. The
730 last term represents the cerebellar feedback. Here $z(t)$ is a 2-dimensional vector
731 encoding the coordinates of the target on the target plane. In our model, the
732 cerebellar feedback is a simple linear transformation of the cortical activity

733 (13) $$z(t) = W^{ro} r(t).$$

734 where the 2-by-*N* cortical readout matrix W^{ro} is trained to produce the correct target
735 in z using linear regression in an open loop model (i.e., setting z to the correct values
736 in equation (13) and learning W^{ro} through linear regression from the mean activity of
737 $r(t)$ in for each target. The model has three parameters: the amount of disorder g,
738 the efficacy of the unstructured input α, and the efficacy of the structured feedback

β. Cerebellar blocking was simulated by reducing the efficacy of the structured feedback β. We trained the readout W^{ro} for each value of β, indicating adaptation to the cerebellar blockage. For each value, we calculated the PCA dimension and CCGP of the cortical activity using the full cortical population. In the model, β remained finite even during "HFS" trials, thus corresponding to the task structure learned by the cortex through other connected areas (e.g., the Basal Ganglia), or incomplete blockage of the cerebellar output. We repeated the simulation 600 times. In each simulation we randomly samples the cortical connectivity (W^{ctx}), the cerebellar and external input (W^{crb} and W^{ex}), and learned the appropriate readout matrix (W^{ro}).

Statistical analyses

All the behavioral data and single cell analyses were conducted using MATLAB software (Mathworks). Differences between adaptation in the control and HFS conditions were assessed using two-way ANOVAs, with learning bins as one factor and the presence or absence of HFS as the other factor. Comparisons of the correlations between deviations and trial number were made using a Wilcoxon rank sum test. Comparisons of learning indices (LIs) in catch trials and error sensitivity at different noise levels implemented two-way ANOVAs. Comparisons of generalization across stimulation conditions was assessed by two-way ANOVA. In all comparisons, the significance level was set at 0.05.

Acknowledgments

This work was funded by the Israel Science Foundation (ISF-1207/23 to Y.P., ISF-1821/23 to J.K. and ISF-2484/23 for F.M.), the Deutsche Forschungsgemeinschaft (431549029-SFB 1451 to Y.P.), the BSF (2019229 for Y.P. and 2021323 for F.M.) and the generous support of the Baruch Foundation (to Y.P.) and the Azrieli Foundation (to J.K.).

Autor information

These authors contributed equally: Sharon Israeli and Hugo Ninou

Authors and Affiliations

The Edmond and Lily Safra Center For Brain Sciences, The Hebrew University, Jerusalem, 91904-01, Israel
Sharon Israeli, Hugo Ninou, Jonathan Kadmon & Yifat Prut
Faculty of Biomedical Engineering, Technion - Israel Institute of Technology, Haifa, Israel
Ori Rejchert & Firas Mawase
Department of Neurosurgery, Sheba Medical Center, 5262000 Tel Aviv, Israel
Ran Harel

Hugo Ninou's present address: Laboratoire de Neurosciences Cognitives et Computationnelles, INSERM U960, Département D'Etudes Cognitives, Ecole Normale Supérieure, PSL University, Paris, France, Laboratoire de Physique de l'Ecole Normale Superieure, Ecole Normale Supérieure, PSL University, Paris, France

Contributions

Y.P. conceived the project. S.I. and R.H. run the experiments. S.I. collected the data. S.I., H.N., and O.R. analyzed the data. L.E. simulated the computational model. F.M., J.K. and Y.P. supervised the project. J.K., H.N., S.I. and Y.P. wrote the original draft of the paper.

Corresponding authors

Correspondence to Yifat Prut and Jonathan Kadmon

References

1 Krakauer, J. W., Hadjiosif, A. M., Xu, J., Wong, A. L. & Haith, A. M. Motor Learning. *Compr Physiol* **9**, 613-663 (2019). https://doi.org:10.1002/cphy.c170043
2 Shadmehr, R., Smith, M. A. & Krakauer, J. W. Error correction, sensory prediction, and adaptation in motor control. *Annual review of neuroscience* **33**, 89-108 (2010). https://doi.org:10.1146/annurev-neuro-060909-153135
3 Kawato, M. Internal models for motor control and trajectory planning. *Current opinion in neurobiology* **9**, 10 (1999).
4 Wolpert, D. M., Miall, R. C. & Kawato, M. Internal models in the cerebellum. *Trends in cognitive sciences* **2**, 10 (1998).
5 Chen, H., Hua, S. E., Smith, M. A., Lenz, F. A. & Shadmehr, R. Effects of human cerebellar thalamus disruption on adaptive control of reaching. *Cereb Cortex* **16**, 1462-1473 (2006). https://doi.org:10.1093/cercor/bhj087

6 Herzfeld, D. J., Kojima, Y., Soetedjo, R. & Shadmehr, R. Encoding of error and learning to correct that error by the Purkinje cells of the cerebellum. *Nature neuroscience* **21**, 736-743 (2018). https://doi.org:10.1038/s41593-018-0136-y

7 Pasalar, S., Roitman, A. V., Durfee, W. K. & Ebner, T. J. Force field effects on cerebellar Purkinje cell discharge with implications for internal models. *Nature neuroscience* **9**, 1404-1411 (2006). https://doi.org:10.1038/nn1783

8 Thoroughman, K. A. & Shadmehr, R. Learning of action through adaptive combination of motor primitives. *Nature* **407**, 742-747 (2000). https://doi.org:10.1038/35037588

9 Giovannucci, A. *et al.* Cerebellar granule cells acquire a widespread predictive feedback signal during motor learning. *Nature neuroscience* **20**, 727-734 (2017). https://doi.org:10.1038/nn.4531

10 Heffley, W. *et al.* Coordinated cerebellar climbing fiber activity signals learned sensorimotor predictions. *Nature neuroscience* **21**, 1431-1441 (2018). https://doi.org:10.1038/s41593-018-0228-8

11 Streng, M. L., Popa, L. S. & Ebner, T. J. Modulation of sensory prediction error in Purkinje cells during visual feedback manipulations. *Nat Commun* **9**, 1099 (2018). https://doi.org:10.1038/s41467-018-03541-0

12 Nezafat, R., Shadmehr, R. & Holcomb, H. H. Long-term adaptation to dynamics of reaching movements: a PET study. *Experimental brain research* **140**, 66-76 (2001). https://doi.org:10.1007/s002210100787

13 Hulst, T. *et al.* Cerebellar patients do not benefit from cerebellar or M1 transcranial direct current stimulation during force-field reaching adaptation. *Journal of neurophysiology* **118**, 732-748 (2017). https://doi.org:10.1152/jn.00808.2016

14 Lang, C. E. & Bastian, A. J. Cerebellar subjects show impaired adaptation of anticipatory EMG during catching. *Journal of neurophysiology* **82**, 2108-2119 (1999). https://doi.org:DOI 10.1152/jn.1999.82.5.2108

15 Morton, S. M. & Bastian, A. J. Cerebellar contributions to locomotor adaptations during splitbelt treadmill walking. *The Journal of neuroscience : the official journal of the Society for Neuroscience* **26**, 9107-9116 (2006). https://doi.org:10.1523/JNEUROSCI.2622-06.2006

16 Nowak, D. A., Hermsdorfer, J., Rost, K., Timmann, D. & Topka, H. Predictive and reactive finger force control during catching in cerebellar degeneration. *Cerebellum* **3**, 227-235 (2004). https://doi.org:10.1080/14734220410019057

17 Panouilleres, M. *et al.* Effects of structural and functional cerebellar lesions on sensorimotor adaptation of saccades. *Experimental brain research* **231**, 1-11 (2013). https://doi.org:10.1007/s00221-013-3662-6

18 Statton, M. A., Vazquez, A., Morton, S. M., Vasudevan, E. V. L. & Bastian, A. J. Making Sense of Cerebellar Contributions to Perceptual and Motor Adaptation. *Cerebellum* **17**, 111-121 (2018). https://doi.org:10.1007/s12311-017-0879-0

19 Horne, M. & Butler, E. The role of the cerebello-thalamo-cortical pathway in skilled movement. *Prog Neurobiol* **46**, 199-213 (1995).

20 Ebrahimi, S. & Ostry, D. J. The human somatosensory cortex contributes to the encoding of newly learned movements. *Proceedings of the National Academy of*

Sciences of the United States of America **121**, e2316294121 (2024). https://doi.org:10.1073/pnas.2316294121

21 Mathis, M. W., Mathis, A. & Uchida, N. Somatosensory Cortex Plays an Essential Role in Forelimb Motor Adaptation in Mice. *Neuron* **93**, 1493-1503 e1496 (2017). https://doi.org:10.1016/j.neuron.2017.02.049

22 Paz, R., Boraud, T., Natan, C., Bergman, H. & Vaadia, E. Preparatory activity in motor cortex reflects learning of local visuomotor skills. *Nature neuroscience* **6**, 882-890 (2003). https://doi.org:10.1038/nn1097

23 Perich, M. G., Gallego, J. A. & Miller, L. E. A Neural Population Mechanism for Rapid Learning. *Neuron* **100**, 964-976 e967 (2018). https://doi.org:10.1016/j.neuron.2018.09.030

24 Peters, A. J., Lee, J., Hedrick, N. G., O'Neil, K. & Komiyama, T. Reorganization of corticospinal output during motor learning. *Nature neuroscience* **20**, 1133-1141 (2017). https://doi.org:10.1038/nn.4596

25 Sun, X. *et al.* Cortical preparatory activity indexes learned motor memories. *Nature* **602**, 274-279 (2022). https://doi.org:10.1038/s41586-021-04329-x

26 Vyas, S. *et al.* Neural Population Dynamics Underlying Motor Learning Transfer. *Neuron* **97**, 1177-1186 e1173 (2018). https://doi.org:10.1016/j.neuron.2018.01.040

27 Chabrol, F. P., Blot, A. & Mrsic-Flogel, T. D. Cerebellar Contribution to Preparatory Activity in Motor Neocortex. *Neuron* **103**, 506-519 e504 (2019). https://doi.org:10.1016/j.neuron.2019.05.022

28 Gao, Z. *et al.* A cortico-cerebellar loop for motor planning. *Nature* **563**, 113-116 (2018). https://doi.org:10.1038/s41586-018-0633-x

29 Zhu, J., Hasanbegovic, H., Liu, L. D., Gao, Z. & Li, N. Activity map of a cortico-cerebellar loop underlying motor planning. *Nature neuroscience* **26**, 1916-1928 (2023). https://doi.org:10.1038/s41593-023-01453-x

30 Nashef, A., Cohen, O., Harel, R., Israel, Z. & Prut, Y. Reversible Block of Cerebellar Outflow Reveals Cortical Circuitry for Motor Coordination. *Cell Rep* **27**, 2608-2619 e2604 (2019). https://doi.org:10.1016/j.celrep.2019.04.100

31 Gibo, T. L., Criscimagna-Hemminger, S. E., Okamura, A. M. & Bastian, A. J. Cerebellar motor learning: are environment dynamics more important than error size? *Journal of neurophysiology* **110**, 322-333 (2013). https://doi.org:10.1152/jn.00745.2012

32 Schlerf, J. E., Xu, J., Klemfuss, N. M., Griffiths, T. L. & Ivry, R. B. Individuals with cerebellar degeneration show similar adaptation deficits with large and small visuomotor errors. *Journal of neurophysiology* **109**, 1164-1173 (2013). https://doi.org:10.1152/jn.00654.2011

33 Criscimagna-Hemminger, S. E., Donchin, O., Gazzaniga, M. S. & Shadmehr, R. Learned dynamics of reaching movements generalize from dominant to nondominant arm. *Journal of neurophysiology* **89**, 168-176 (2003). https://doi.org:10.1152/jn.00622.2002

34 Vyas, S., O'Shea, D. J., Ryu, S. I. & Shenoy, K. V. Causal Role of Motor Preparation during Error-Driven Learning. *Neuron* **106**, 329-339 e324 (2020). https://doi.org:10.1016/j.neuron.2020.01.019

35 Wolpert, D. M., Ghahramani, Z. & Jordan, M. I. An internal model for sensorimotor integration. *Science* **269**, 1880-1882 (1995). https://doi.org:10.1126/science.7569931

36 Herzfeld, D. J., Vaswani, P. A., Marko, M. K. & Shadmehr, R. A memory of errors in sensorimotor learning. *Science* **345**, 1349-1353 (2014). https://doi.org:10.1126/science.1253138

37 Albert, S. T. *et al.* An implicit memory of errors limits human sensorimotor adaptation. *Nat Hum Behav* **5**, 920-934 (2021). https://doi.org:10.1038/s41562-020-01036-x

38 Mante, V., Sussillo, D., Shenoy, K. V. & Newsome, W. T. Context-dependent computation by recurrent dynamics in prefrontal cortex. *Nature* **503**, 78-84 (2013). https://doi.org:10.1038/nature12742

39 Gao, P. *et al.* A theory of multineuronal dimensionality, dynamics and measurement. *bioRxiv* (2017). https://doi.org:https://doi.org/10.1101/214262

40 Mazzucato, L., Fontanini, A. & La Camera, G. Stimuli Reduce the Dimensionality of Cortical Activity. *Frontiers in systems neuroscience* **10**, 11 (2016). https://doi.org:10.3389/fnsys.2016.00011

41 Bernardi, S. *et al.* The Geometry of Abstraction in the Hippocampus and Prefrontal Cortex. *Cell* **183**, 954-967 e921 (2020). https://doi.org:10.1016/j.cell.2020.09.031

42 Johnston, W. J. & Fusi, S. Abstract representations emerge naturally in neural networks trained to perform multiple tasks. *Nat Commun* **14**, 1040 (2023). https://doi.org:10.1038/s41467-023-36583-0

43 Boven, E., Pemberton, J., Chadderton, P., Apps, R. & Costa, R. P. Cerebro-cerebellar networks facilitate learning through feedback decoupling. *Nat Commun* **14**, 51 (2023). https://doi.org:10.1038/s41467-022-35658-8

44 Sokolov, A. A., Miall, R. C. & Ivry, R. B. The Cerebellum: Adaptive Prediction for Movement and Cognition. *Trends in cognitive sciences* **21**, 313-332 (2017). https://doi.org:10.1016/j.tics.2017.02.005

45 Maschke, M., Gomez, C. M., Ebner, T. J. & Konczak, J. Hereditary cerebellar ataxia progressively impairs force adaptation during goal-directed arm movements. *Journal of neurophysiology* **91**, 230-238 (2004). https://doi.org:10.1152/jn.00557.2003

46 Richter, S. *et al.* Adaptive motor behavior of cerebellar patients during exposure to unfamiliar external forces. *J Mot Behav* **36**, 28-38 (2004). https://doi.org:10.3200/JMBR.36.1.28-38

47 Taylor, J. A., Klemfuss, N. M. & Ivry, R. B. An explicit strategy prevails when the cerebellum fails to compute movement errors. *Cerebellum* **9**, 580-586 (2010). https://doi.org:10.1007/s12311-010-0201-x

48 Bastian, A. J. Learning to predict the future: the cerebellum adapts feedforward movement control. *Current opinion in neurobiology* **16**, 645-649 (2006). https://doi.org:10.1016/j.conb.2006.08.016

49 Butcher, P. A. *et al.* The cerebellum does more than sensory prediction error-based learning in sensorimotor adaptation tasks. *Journal of neurophysiology* **118**, 1622-1636 (2017). https://doi.org:10.1152/jn.00451.2017

50 Diedrichsen, J., Hashambhoy, Y., Rane, T. & Shadmehr, R. Neural correlates of reach errors. *The Journal of neuroscience : the official journal of the Society for Neuroscience* **25**, 9919-9931 (2005). https://doi.org:10.1523/JNEUROSCI.1874-05.2005

51 Smith, M. A., Ghazizadeh, A. & Shadmehr, R. Interacting adaptive processes with different timescales underlie short-term motor learning. *PLoS Biol* **4**, e179 (2006). https://doi.org:10.1371/journal.pbio.0040179

52 Donchin, O. *et al.* Cerebellar regions involved in adaptation to force field and visuomotor perturbation. *Journal of neurophysiology* **107**, 134-147 (2012). https://doi.org:10.1152/jn.00007.2011

53 Smith, M. A. & Shadmehr, R. Intact ability to learn internal models of arm dynamics in Huntington's disease but not cerebellar degeneration. *Journal of neurophysiology* **93**, 2809-2821 (2005). https://doi.org:10.1152/jn.00943.2004

54 Taig, E., Kuper, M., Theysohn, N., Timmann, D. & Donchin, O. Deficient use of visual information in estimating hand position in cerebellar patients. *The Journal of neuroscience : the official journal of the Society for Neuroscience* **32**, 16274-16284 (2012). https://doi.org:10.1523/JNEUROSCI.1153-12.2012

55 Gallego, J. A., Perich, M. G., Miller, L. E. & Solla, S. A. Neural Manifolds for the Control of Movement. *Neuron* **94**, 978-984 (2017). https://doi.org:10.1016/j.neuron.2017.05.025

56 Gallego, J. A. *et al.* Cortical population activity within a preserved neural manifold underlies multiple motor behaviors. *Nat Commun* **9**, 4233 (2018). https://doi.org:10.1038/s41467-018-06560-z

57 Sadtler, P. T. *et al.* Neural constraints on learning. *Nature* **512**, 423-426 (2014). https://doi.org:10.1038/nature13665

58 Malfait, N. & Ostry, D. J. Is interlimb transfer of force-field adaptation a cognitive response to the sudden introduction of load? *The Journal of neuroscience : the official journal of the Society for Neuroscience* **24**, 8084-8089 (2004). https://doi.org:10.1523/JNEUROSCI.1742-04.2004

59 Howard, I. S. & Franklin, D. W. Neural Tuning Functions Underlie Both Generalization and Interference. *PLoS One* **10**, e0131268 (2015). https://doi.org:10.1371/journal.pone.0131268

60 Shadmehr, R. Generalization as a behavioral window to the neural mechanisms of learning internal models. *Hum Mov Sci* **23**, 543-568 (2004). https://doi.org:10.1016/j.humov.2004.04.003

61 Person, A. L. Corollary Discharge Signals in the Cerebellum. *Biol Psychiatry Cogn Neurosci Neuroimaging* **4**, 813-819 (2019). https://doi.org:10.1016/j.bpsc.2019.04.010

62 Kostadinov, D., Beau, M., Blanco-Pozo, M. & Hausser, M. Predictive and reactive reward signals conveyed by climbing fiber inputs to cerebellar Purkinje cells. *Nature neuroscience* **22**, 950-962 (2019). https://doi.org:10.1038/s41593-019-0381-8

63 Mussells Pires, P., Zhang, L., Parache, V., Abbott, L. F. & Maimon, G. Converting an allocentric goal into an egocentric steering signal. *Nature* **626**, 808-818 (2024). https://doi.org:10.1038/s41586-023-07006-3

64 Nashef, A., Cohen, O., Perlmutter, S. I. & Prut, Y. A cerebellar origin of feedforward inhibition to the motor cortex in non-human primates. *Cell Rep* **39**, 110803 (2022). https://doi.org:10.1016/j.celrep.2022.110803

65 Nashef, A., Mitelman, R., Harel, R., Joshua, M. & Prut, Y. Area-specific thalamocortical synchronization underlies the transition from motor planning to execution. *Proceedings of the National Academy of Sciences of the United States of America* **118** (2021). https://doi.org:10.1073/pnas.2012658118

66 Nashef, A., Cohen, O., Israel, Z., Harel, R. & Prut, Y. Cerebellar Shaping of Motor Cortical Firing Is Correlated with Timing of Motor Actions. *Cell Rep* **23**, 1275-1285 (2018). https://doi.org:10.1016/j.celrep.2018.04.035

67 Ruach, R., Mitelman, R., Sherman, E., Cohen, O. & Prut, Y. An assumption-free quantification of neural responses to electrical stimulations. *J Neurosci Meth* (2015). https://doi.org:10.1016/j.jneumeth.2015.07.005

68 Kadmon, J., Timcheck, J. & Ganguli, S. Predictive coding in balanced neural networks with noise, chaos and delays. *Advances in neural information processing systems* **33**, 16677-16688 (2020).

69 Timcheck, J., Kadmon, J., Boahen, K. & Ganguli, S. Optimal noise level for coding with tightly balanced networks of spiking neurons in the presence of transmission delays. *PLoS Comput Biol* **18**, e1010593 (2022). https://doi.org:10.1371/journal.pcbi.1010593

70 Amari, S. I. Learning Patterns and Pattern Sequences by Self-Organizing Nets of Threshold Elements. *Ieee T Comput* **C 21**, 1197-+ (1972). https://doi.org:Doi 10.1109/T-C.1972.223477

1011 **Supplemental material**

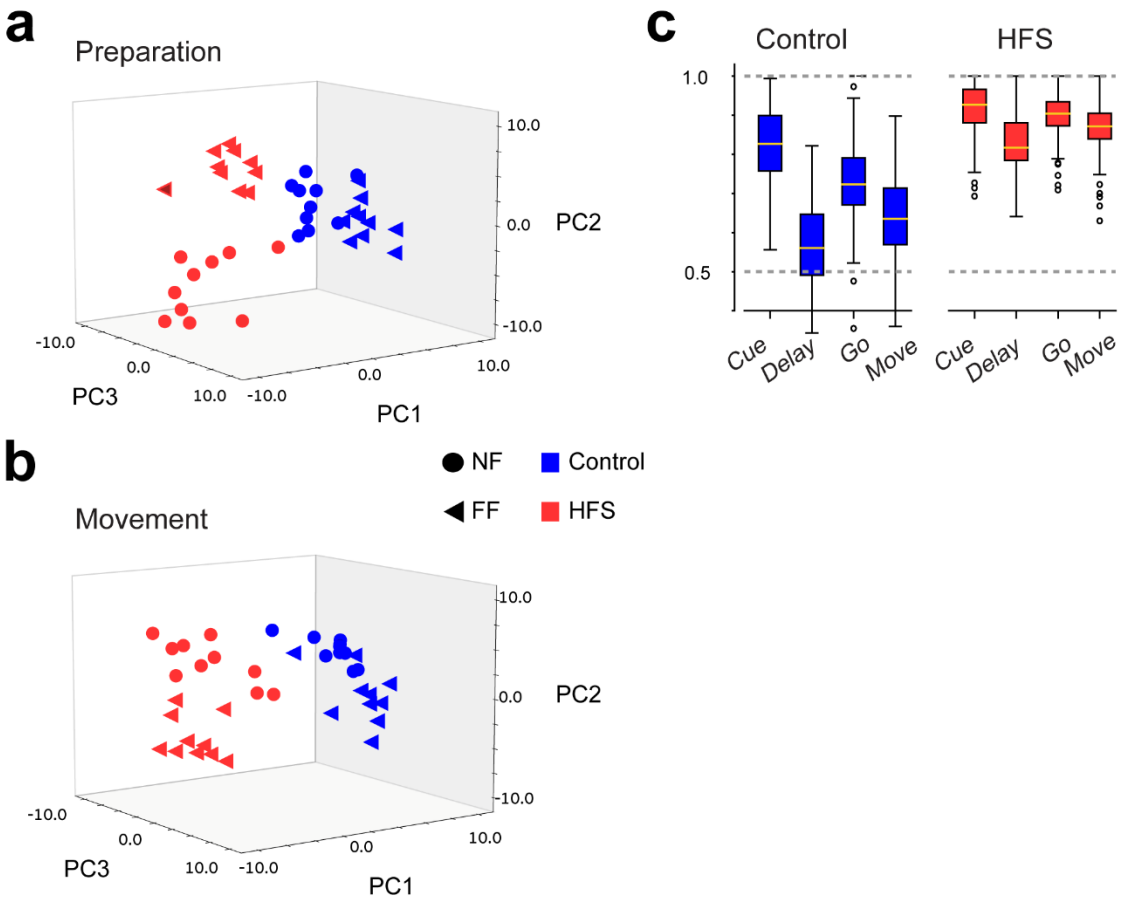

Supplementary Figure 1. Single-trial projection decoding accuracy calculated for Monkey P. Unlike Monkey S (Fig. 4a-c), here we only had 10 trials for the 4 different conditions. **a,** Projection of trial-specific coordinated activity on the first 3 PCs during preparation for movement. Each dot represents coordinated activity in a single trial during the sequence of trials performed in control (blue) or HFS (red) conditions, either before adaptation (null field, NF - circles) or during adaptation (FF - triangles). Neural data were averaged across all targets and obtained during a time window spanning -300 ms to 0 around the Go signal. **b,** Same as a but calculated during the 100-400 ms after the Go signal. **c,** Decoding accuracy of adaptation conditions (NF vs. FF) based on epoch-specific data for the control (blue bars) or HFS (red bars). The dashed line denotes chance level (0.5). The different values for decoding accuracy were obtained for different realizations of the training and testing sets.

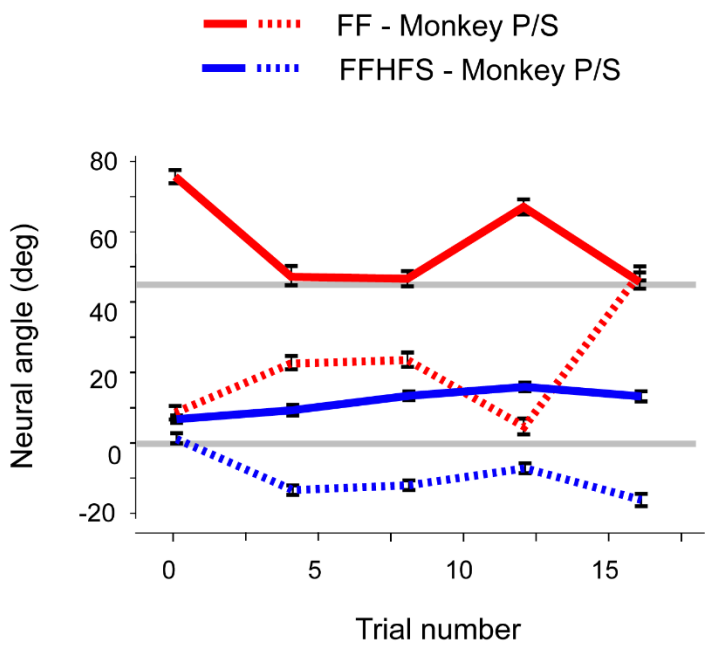

Supplementary Figure 2. Neural angle as a function of trial number. Average neural angle as a function of the trial number, ordered from early trials (with high maximal deviation values) to late trials (with low maximal deviations). Neural angles for monkeys P and S are shown respectively in full and dashed lines. Blue and red, respectively indicate the FF and FF-HFS conditions.

1012

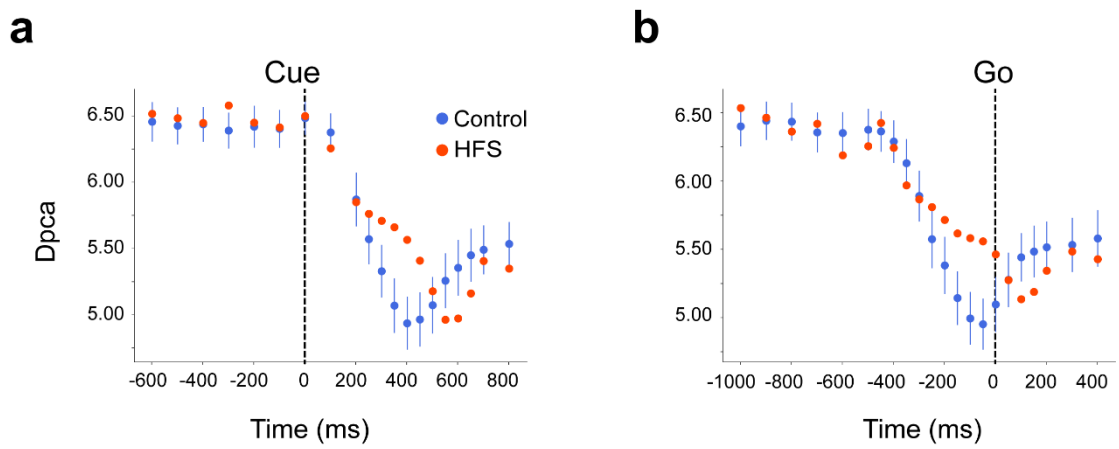

Supplementary Figure 3. Time-resolved modulation of participation ratio (Dpca). The Dpca was calculated (see Methods) in time bins of 5 ms, sampled every 100 ms. Calculations were performed on data aligned on the Cue (**a**) or the Go (**b**) events. Since in almost all cases there were more trials available in the Control than in the HFS conditions, we used a resampling method on the control data to obtain confidence intervals, shown as bars around control data (corresponding to the standard deviations).